Molecular Cell

Article

CDK4/6 inhibitor-mediated cell overgrowth triggers osmotic and replication stress to promote senescence

Graphical abstract

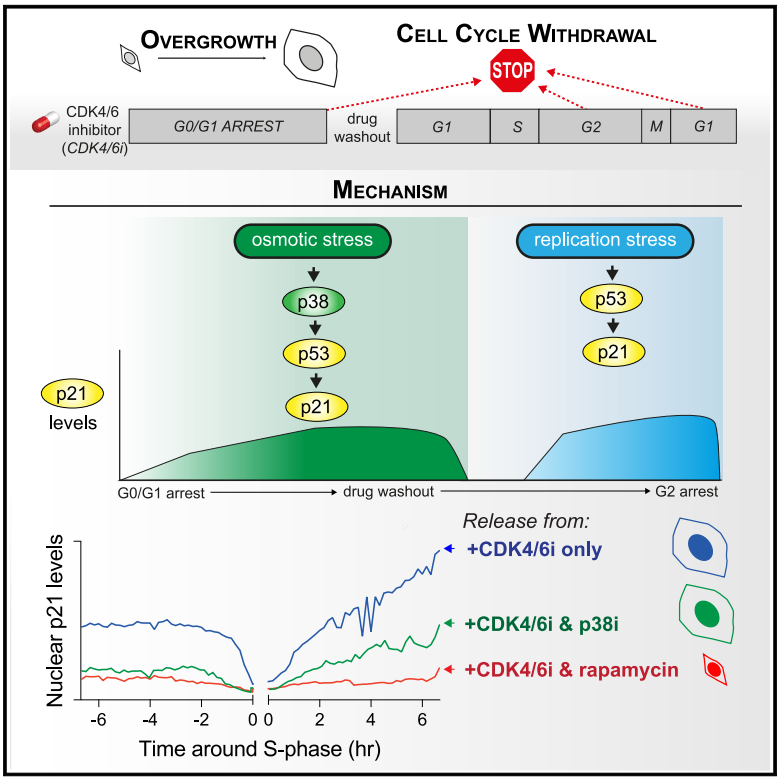

Highlights

- Cell overgrowth during CDK4/6-inhibitor-mediated G0/G1 arrest promotes senescence
- Overgrowth initiates an osmotic stress response driving p38/p53/p21 signaling
- High p21 protein maintains the G0/G1 arrest after CDK4/6-inhibitor washout
- Escapees experience replication stress and p21-dependent cell-cycle exit

Authors

Lisa Crozier, Reece Foy, Rozita Adib, ..., Adrian T. Saurin, Alexis R. Barr, Tony Ly

Correspondence

a.saurin@dundee.ac.uk (A.T.S.), a.barr@lms.mrc.ac.uk (A.R.B.), t.ly@dundee.ac.uk (T.L.)

In brief

CDK4/6 inhibitors, used to treat metastatic breast cancer, can have long-term anti-proliferative effects, even after patients finish treatment. Crozier et al. show that CDK4/6 inhibitors block cell proliferation but not growth. This causes cell overgrowth, leading to biphasic cellular stress responses that drive permanent cell-cycle withdrawal.

Crozier et al., 2023, Molecular Cell *83*, 4062–4077
November 16, 2023
https://doi.org/10.1016/j.molcel.2023.10.016

CellPress

CellPress
OPEN ACCESS

Molecular Cell

Article

CDK4/6 inhibitor-mediated cell overgrowth triggers osmotic and replication stress to promote senescence

Lisa Crozier,[1,9] Reece Foy,[1,9] Rozita Adib,[2,9] Ananya Kar,[3] Jordan A. Holt,[2] Aanchal U. Pareri,[1] Juan M. Valverde,[1] Rene Rivera,[3] William A. Weston,[2] Rona Wilson,[4] Clement Regnault,[5] Phil Whitfield,[5] Mihaly Badonyi,[6] Laura G. Bennett,[7] Ellen G. Vernon,[7] Amelia Gamble,[7] Joseph A. Marsh,[6] Christopher J. Staples,[7] Adrian T. Saurin,[1,*] Alexis R. Barr,[2,8,*] and Tony Ly[3,4,5,10,*]

[1]Cellular and Systems Medicine, Jacqui Wood Cancer Centre, School of Medicine, University of Dundee, Dundee, UK
[2]MRC Laboratory of Medical Sciences, London, UK
[3]Molecular Cell and Developmental Biology, School of Life Sciences, Dundee, UK
[4]Wellcome Centre for Cell Biology, University of Edinburgh, Edinburgh, UK
[5]Glasgow Polyomics College of Medical, Veterinary, and Life Sciences, University of Glasgow, UK
[6]MRC Human Genetics Unit, University of Edinburgh, Edinburgh, UK
[7]North West Cancer Research Institute, School of Medical and Health Sciences, Brambell Building, Deiniol Rd, Bangor LL57 2UW, UK
[8]Institute of Clinical Sciences, Faculty of Medicine, Imperial College London, London, UK
[9]These authors contributed equally
[10]Lead contact
*Correspondence: a.saurin@dundee.ac.uk (A.T.S.), a.barr@lms.mrc.ac.uk (A.R.B.), t.ly@dundee.ac.uk (T.L.)
https://doi.org/10.1016/j.molcel.2023.10.016

SUMMARY

Abnormal increases in cell size are associated with senescence and cell cycle exit. The mechanisms by which overgrowth primes cells to withdraw from the cell cycle remain unknown. We address this question using CDK4/6 inhibitors, which arrest cells in G0/G1 and are licensed to treat advanced HR+/HER2− breast cancer. We demonstrate that CDK4/6-inhibited cells overgrow during G0/G1, causing p38/p53/p21-dependent cell cycle withdrawal. Cell cycle withdrawal is triggered by biphasic p21 induction. The first p21 wave is caused by osmotic stress, leading to p38- and size-dependent accumulation of p21. CDK4/6 inhibitor washout results in some cells entering S-phase. Overgrown cells experience replication stress, resulting in a second p21 wave that promotes cell cycle withdrawal from G2 or the subsequent G1. We propose that the levels of p21 integrate signals from overgrowth-triggered stresses to determine cell fate. This model explains how hypertrophy can drive senescence and why CDK4/6 inhibitors have long-lasting effects in patients.

INTRODUCTION

The success of CDK4/6 inhibitors (CDK4/6i) in treating hormone-receptor positive (HR+), human epidermal growth factor receptor 2 negative (HER2−) metastatic breast cancer[1–3] has reinvigorated interest in targeting cell cycle entry pathways for cancer treatment.[4,5] CDK4/6 and D-type cyclins form active kinase complexes that phosphorylate retinoblastoma protein (Rb)[6] to promote G0-G1 progression and S-phase entry.[7] CDK4/6 inhibition results in hypophosphorylated Rb, which suppresses transcription of cell cycle genes. Results from the clinic, animal models, and *in vitro* suggest that the mechanisms of action of CDK4/6 inhibition are complex.[8–11] For example, although the high frequency of resistance-driving genetic lesions in RB1 was expected, the mechanisms of how other genetic lesions drive CDK4/6i resistance cannot be so easily explained.[12,13] CDK4/6i have unanticipated effects on the immune system,[14–17] and tumor cell clearance in animal models is dependent on T cell function.[15] Thus, major gaps exist in our current understanding of the molecular mechanisms of CDK4/6i-mediated tumor cell clearance.

Prolonged treatment with CDK4/6i can promote cellular senescence across a range of cell types and *in vivo*.[8,18,19] CDK4/6i-treated cells arrest in G0/G1 but continue to accumulate biomass and increase in cell volume.[20–22] Continued cell growth contributes to the onset of permanent cell cycle arrest and senescent phenotypes.[23] However, the mechanisms linking excessive cellular growth to permanent cell cycle arrest are poorly characterized. One model suggests an abnormal DNA:cytoplasm ratio in excessively large cells promotes permanent cell cycle arrest.[21] Downstream, permanent cell cycle arrest after prolonged CDK4/6 inhibition has been demonstrated to be p53-dependent.[18,24] How cells sense either abnormal cell size, or an abnormal DNA:cytoplasm ratio, and the molecular pathways that link cell overgrowth to p53 activity are not understood.[25]

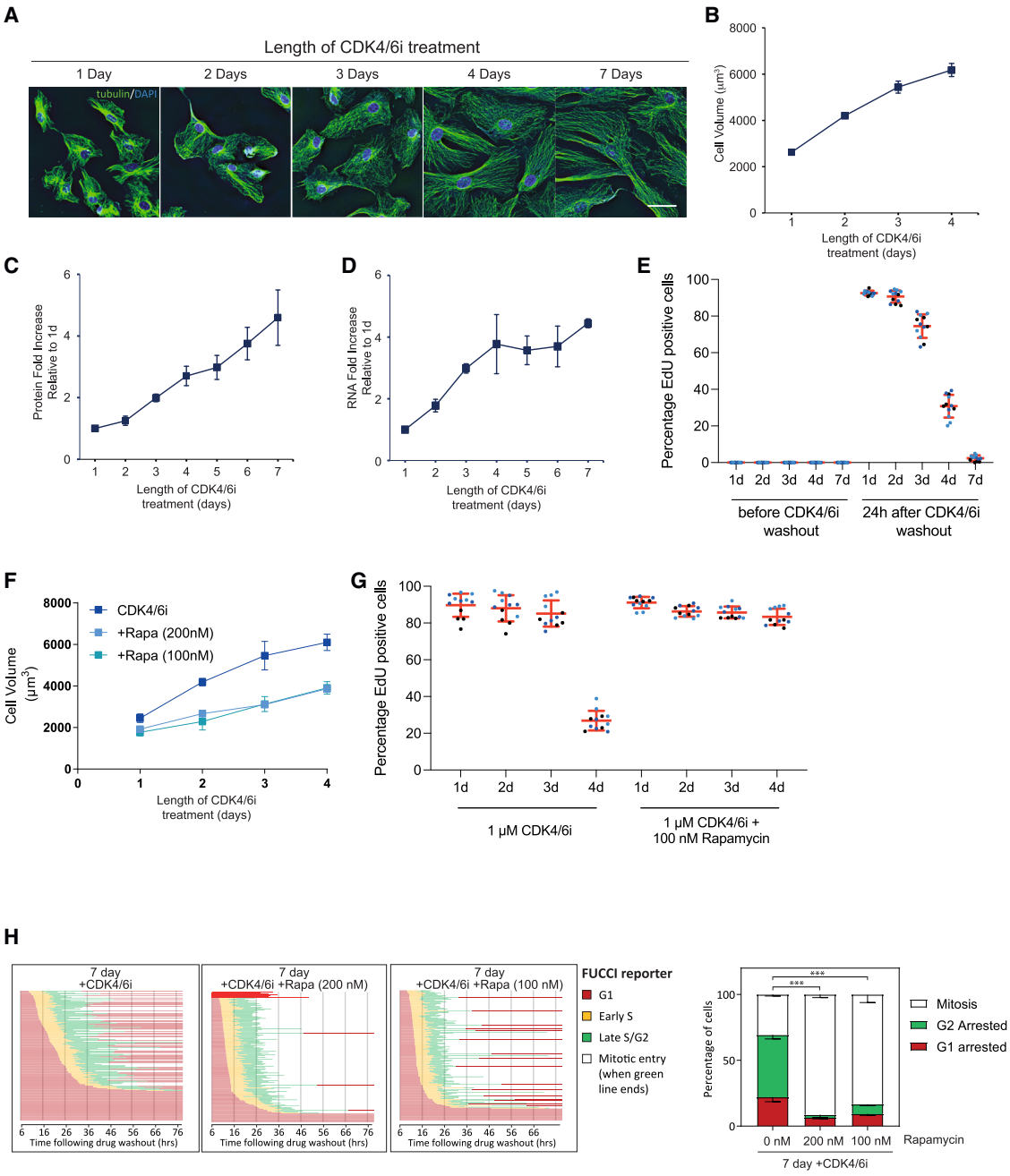

Figure 1. Long-term CDK4/6i treatment promotes cellular overgrowth that drives permanent cell cycle arrest

(A) Images of RPE1 cells incubated in CDK4/6i for increasing time. Green is alpha-tubulin and blue is 4',6-diamidino-2-phenylindole (DAPI) to label nuclei. Scale bar, 50 µm.

(B–D) Cells grow during a prolonged CDK4/6i arrest shown by increases in cell volume (B), protein content (C), and RNA content (D). Mean of n = 2 ± SD. Note, in (B) cell volume is only measured up to 4 days of CDK4/6i treatment. This is because CDK4/6i-treated RPE1 cells do not round up properly after trypsinisation beyond 4 days, making accurate cell volume measurements challenging.

(E) Percentage of RPE1 mRuby-PCNA cells re-entering S-phase (EdU positive) after increasing days of 1 µM CDK4/6i treatment followed by 24 h washout into fresh media containing EdU. Data are plotted as superplots, where each technical repeat is a single dot and biological repeats are in different colors. Mean ± SD of n = 3 are shown in red.

(F) Co-treatment of cells with CDK4/6i and rapamycin inhibits cell growth during the prolonged arrest. Mean of n = 3 ± SD are shown.

(G) Co-treatment of cells with CDK4/6i and rapamycin allows cells to maintain proliferative potential during the prolonged arrest. Data are plotted as superplots. Mean ± SD of n = 3 are shown in red.

(legend continued on next page)

Here, we demonstrate that permanent cell cycle arrest is caused by excessive cell growth during the G0/G1 arrest. We have combined fixed and live quantitative single-cell imaging with quantitative proteomics and perturbation experiments to characterize the molecular mechanisms of permanent cell cycle arrest. We show that prolonged CDK4/6i treatment promotes cell overgrowth, a cell state characterized by abnormally large size and increased p21 levels, downstream of p53 activation by osmotic and replication stress. Our work establishes how cells can sense cellular overgrowth, for example, driven by growth-promoting oncogenes and withdraw from the cell cycle. This is likely important for HR+/HER2− breast cancers treated with CDK4/6i, especially since these cells are often p53 proficient and, as shown in an accompanying paper by Foy et al.,[26] they contain oncogenes that prime overgrowth during the G0/G1 arrest.

RESULTS

Long-term CDK4/6i treatment promotes cellular overgrowth that drives permanent cell cycle arrest

Treatment of non-transformed hTERT-RPE1 (RPE1) and ER+ breast cancer MCF7 cells with the CDK4/6i, Palbociclib, causes cells to arrest in G0/G1.[24,27] Prolonged treatment of RPE1 or MCF7 cells with CDK4/6i was accompanied by an increase in cell size that correlated with the length of CDK4/6i treatment (Figures 1A, 1B, and S1A–S1E). This increase in cell size was accompanied by increases in cellular protein and RNA content (Figures 1C and 1D). Previous work showed that S-phase re-entry after CDK4/6i washout declines after 2 days of CDK4/6i treatment.[24,27] Consistent with this, we observed S-phase re-entry negatively correlates with CDK4/6i treatment duration and cell size (Figures 1E and S1G).

To investigate if the cell size increase causes reduced S-phase re-entry after CDK4/6i washout, we treated cells with CDK4/6i under conditions that restricted cell growth. mTOR is a master regulator of cell growth and co-treatment with rapamycin, an inhibitor of mTORC1 activity, reduced cell growth during CDK4/6i treatment in both RPE1 and MCF7 cells (Figures 1F and S1F). Indeed, co-treatment with CDK4/6i and rapamycin restored the ability of cells to re-enter S-phase after inhibitor washout, suggesting that cell overgrowth is the main driver of long-term G0/G1 arrest after CDK4/6i washout (Figures 1G and S1G) and not CDK4/6i treatment duration *per se*.[24]

To understand cell cycle behavior after CDK4/6i washout, we used the FUCCI cell cycle reporter in RPE1 cells.[28,29] Cells were treated with CDK4/6i, or CDK4/6i plus rapamycin (Figure 1H). Approximately 20% of CDK4/6i-treated RPE1 FUCCI cells remain in a G0/G1 arrest after CDK4/6i washout, and of those cells that did re-enter S-phase, a large fraction withdrew from the cell cycle in S/G2, as previously observed.[24] Preventing cell growth with rapamycin co-treatment allowed more cells to re-enter S-phase, with a shorter G1 and a higher fraction of cells completing G2 and entering mitosis (Figure 1H).

Based on these results, we conclude that continued cellular growth during prolonged G0/G1 arrest by CDK4/6i treatment drives permanent cell cycle arrest. To distinguish this from physiological growth during an unperturbed G1, we suggest that prolonged G0/G1 arrest promotes overgrowth.

Long-term cell cycle arrest induced by cellular overgrowth is p21 dependent

Levels of the CDK inhibitor protein, p21, start to increase after 2 days CDK4/6i treatment,[30] and it has been shown that p53, a key transcription factor for p21, is required for the long-term cell cycle arrest phenotypes observed after prolonged CDK4/6i treatment washout.[18,24] The increase in p21 correlates with the loss of the ability of cells to re-enter S-phase after CDK4/6i washout (Figure 1E) and is p53-dependent (Figure 2A). Furthermore, using quantitative proteomics (see STAR Methods), we observed an increase in p21 protein after CDK4/6i treatment, along with increased expression of additional p53 targets (Figure 2B). Consistent with the proteomics data, western blotting showed p21 increases with total protein content (Figure S2A). p21 inhibits CDK1 and CDK2 by direct, stoichiometric binding. CDK1 and CDK2 remain unchanged or even decrease in large cells (Figure 2C). Thus, the ratio of p21 relative to its inhibitory targets is increasing with cell size.

Imaging of RPE1 mRuby-PCNA p21-GFP cells[31] after addition of DMSO, CDK4/6i, or CDK4/6i plus rapamycin showed a marked increase in p21-GFP expression at approximately 48 h post-CDK4/6i addition (Figures 2D and S2B). This increase in p21-GFP expression coincides with the loss of reversibility of the CDK4/6i-induced arrest after 2 days (Figure 1E). Rapamycin co-treatment attenuates the increased nuclear p21-GFP fluorescence at 48 h. Consistent with this, co-treatment of cells with CDK4/6i and rapamycin prevented the accumulation of p21 protein in total cell extracts (Figure 2E) and nuclear p21 in RPE1 and MCF7 cells (Figures S2C and S2D).

To test whether p21 was required to mediate the long-term G0/G1 arrest after CDK4/6i washout, we treated p21 wild-type and p21 knockout (KO) RPE1 cells[31] with CDK4/6i for 7 days and observed that, after CDK4/6i washout, an increased fraction of p21KO cells were able to re-enter S-phase, compared with p21WT cells (Figure 2F). Using live-cell imaging of p21WT or p21KO RPE1 mRuby-PCNA cells,[32] we observed that p21 loss reduces long-term cell cycle arrest, where, in the absence of p21, all cells enter S-phase after CDK4/6i release, have a shorter G1 and complete multiple mitoses (Figures 2G and S2E).

Our results suggest that cellular overgrowth induced by CDK4/6i is sensed by cells and transduced to promote p21-dependent long-term cell cycle arrest in both G0/G1 and G2.

Biphasic accumulation of p21 drives long-term cell cycle arrest from G0/G1 or G2

p53-dependent p21 accumulation could explain long-term cell cycle arrest in G0/G1 after release from prolonged CDK4/6i

(H) Graphs show FUCCI RPE1 cells released from 7-day arrest with indicated inhibitors into the Eg5 inhibitor STLC to arrest cells in mitosis. Live-cell imaging was started 6 h after drug washout. Red is G1, yellow is S-phase, and green is G2. If cells enter mitosis, the bars turn white after G2. In bright red are cells whose fluorescence decreases below detectable range. Cells that withdraw from the cell cycle in G2 return to red color as APC/C^{Cdh1} becomes active and geminin is degraded. Right-hand graph shows mean of n = 3 ± SD. Statistical significance determined by chi-squared test comparing conditions ± rapamycin, ***p < 0.0001.

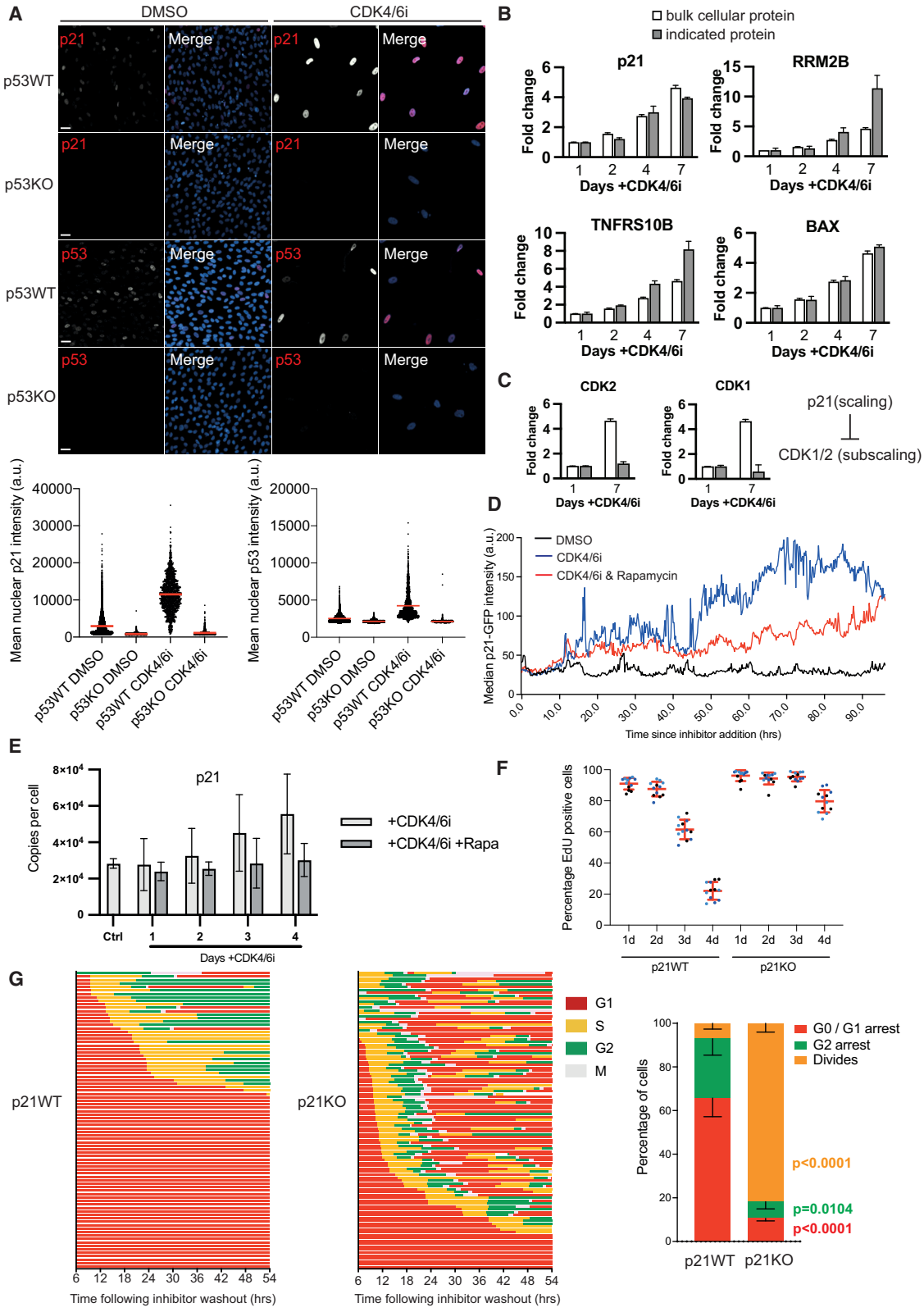

(legend on next page)

treatment because p21 could block CDK activity and prevent cell cycle re-entry. However, in the fraction of cells that re-enter S-phase after CDK4/6i washout, we wanted to know how p21 could drive cell cycle withdrawal from G2 (Figures 1H and 2G).

We imaged RPE1 mRuby-PCNA p21-GFP cells after washout of 7-day CDK4/6i treatment to quantify p21-GFP expression after release (Figure 3A). In cells that remain arrested in G0/G1, p21-GFP levels remain high (red curves, Figures 3A, 3C, and S3A). In cells that re-enter S-phase, p21-GFP is degraded, immediately prior to S-phase entry,[33,34] and is then re-expressed as cells enter G2, leading to a second wave of p21 expression (blue curves, Figures 3A, 3C, and S3A). In cells treated with CDK4/6i plus rapamycin, p21-GFP levels are lower at the time of release (0 h), most cells re-enter S-phase (blue curves, Figure 3B) and, although p21-GFP does start to accumulate in some cells after S-phase exit, the overall levels are lower than those observed after treatment with CDK4/6i only (red curve, Figure 3C), and fewer cells arrest in G2 (Figure 1H).

We hypothesized that cells that remain in G0/G1 after washout of 7-day CDK4/6i treatment would be larger and/or have higher p21 levels than those that re-enter S-phase. We quantified nuclear area and p21-GFP levels immediately after CDK4/6i washout and binned cells into those that remained arrested in G0/G1 (“Arrests,” Figures S3B–S3E) and those that re-entered S-phase (“Enters S,” Figures S3B–S3E). Although we found no significant difference in nuclear area between groups, we did see that p21-GFP levels were significantly lower in cells that re-entered S-phase than those that remain arrested (Figures S3B–S3E). These data suggest that p21 sets a threshold for re-entry into S-phase.

Our data suggest that two waves of p21 expression can promote long-term cell cycle arrest. We have shown that the first wave of p21 accumulation is induced by cellular overgrowth driving p53-dependent p21 expression. Prolonged arrest in CDK4/6i leads to the downregulation of proteins required for DNA origin licensing and DNA replication.[24] This deficiency leads to replication stress in cells that re-enter S-phase after CDK4/6i washout, which could drive p53-dependent p21 expression in G2.[31] If this is the case, we predict that smaller cells (treated with CDK4/6i plus rapamycin) should experience lower levels of replication stress because p21-GFP does not accumulate to as high a level in these G2 cells.

Indeed, co-treatment with rapamycin reduces the amount of DNA damage present in cells 48 h after washout of CDK4/6i (Figures 3D–3F and S3F–S3H). This difference is not due to DNA damage during the G0/G1 arrest because we have no evidence that DNA damage accumulates during 7-day treatment with CDK4/6i.[24] Moreover, we observed reduced replication fork progression when cells were released from 7-day CDK4/6i treatment, which was largely restored when cell overgrowth was inhibited by co-treatment with rapamycin, or a distinct mTOR inhibitor, PF-05212384 (PF-05) (Figures 3G and 3H).[26,35] This effect was also observed in MCF7 cells (Figure S3I). We observed that nucleoside supplementation could restore replication fork progression in cells released from 7-day CDK4/6i treatment (Figures 3H and S3I), suggesting that nucleotides are limiting in overgrown cells.

Our data show that long-term cell cycle arrest is driven by a biphasic p21 response. Cell overgrowth drives p21 accumulation during the prolonged G0/G1 arrest that prevents cells from re-entering S-phase. Then, in cells that re-enter S-phase following CDK4/6i washout, replication stress drives a second wave of p21 expression that promotes cell cycle withdrawal from G2.

Hyperosmotic media suppresses p21 induction during prolonged G0/G1 arrest

The first wave of p21 caused by cellular overgrowth is crucial for G0/G1 arrest, but it is not known what cellular stress(es) induce p21. Indeed, p53-driven p21 expression is activated in response to diverse cellular stresses, including DNA damage,[36,37] reactive oxygen species (ROS),[38] and osmotic stress.[39] We surmised that cell overgrowth triggers one or more of these molecular insults to drive p21 expression.

Markers of DNA damage, including γ-H2AX foci[18,24] and 53BP1 nuclear bodies, do not increase during CDK4/6i-mediated G0/G1 arrest[18,24] (Figure S4A), making nuclear genome damage an unlikely culprit for p21 induction. CDK4/6i treatment increases intracellular ROS (Figure S4B).[40] However, increasing antioxidant capacity by treatment with the ROS scavenging small molecule, N-acetyl cysteine (NAC), fails to prevent p21 induction (Figure S4C). ROS is an umbrella term for multiple chemical species, including superoxide and hydrogen peroxide, which have differing reactivities toward NAC. The NRF2 transcription factor is a master regulator of the cellular antioxidant response,[41]

Figure 2. Long-term cell cycle arrest induced by cellular overgrowth is p21-dependent

(A) Images show representative fields of view of each of the conditions in the graphs. In merged images, p21 or p53 are in red and nuclei are in blue. Scale bars, 20 μm. Graphs show p53 and p21 levels quantified from immunostaining. Each dot represents a single cell. Red bar represents the mean.

(B) Bar graphs showing relative fold change of p53 target proteins in cells treated with CDK4/6i for the indicated number of days (error bars indicate SD).

(C) Bar graphs showing relative fold change CDK1 and CDK2 in cells treated with CDK4/6i for the indicated number of days (error bars indicate SD).

(D) Graph showing nuclear p21-GFP intensity measured in hTert-RPE1 mRuby-PCNA p21-GFP H3.1-iRFP cells after addition of DMSO (black curve), CDK4/6i (blue curve), or CDK4/6i and rapamycin (red curve) to cells. Median p21-GFP intensity of single-cell data are shown: n = 47 for DMSO, n = 78 cells for CDK4/6i, and n = 66 cells for CDK4/6i with rapamycin (single-cell data shown in Figure S2B).

(E) Mean copies of p21 protein in control (untreated and proliferating) cells, cells treated with CDK4/6i, and cells treated with CDK4/6i and rapamycin (+Rapa) (n = 5, error bars indicate SD * indicates $p < 0.05$ from a two-way ANOVA corrected for multiple testing).

(F) Graph showing percentage of cells re-entering S-phase (EdU positive) after CDK4/6i treatment followed by inhibitor washout in p21WTp21KO RPE1 cells. RPE1 cells were arrested in 1 μM CDK4/6i, inhibitor was then washed out and fresh media containing EdU was added. Cells were fixed and analyzed 24 h after inhibitor washout. Data are plotted as superplots mean ± SD of n = 3 are shown in red.

(G) Graphs show timings of cell cycle phases extracted from time-lapse imaging of p21WT or p21KO RPE1 mRuby-PCNA cells, after release and re-plating from 7-day arrest in CDK4/6i. Imaging was started 6 h after washout. Accompanying bar chart shows cell fates after release from inhibitors. “Divides” refers to whether cells complete mitosis after release from inhibitors. Mean ± SD of n = 3 are shown. One-way ANOVA was used to measure significance.

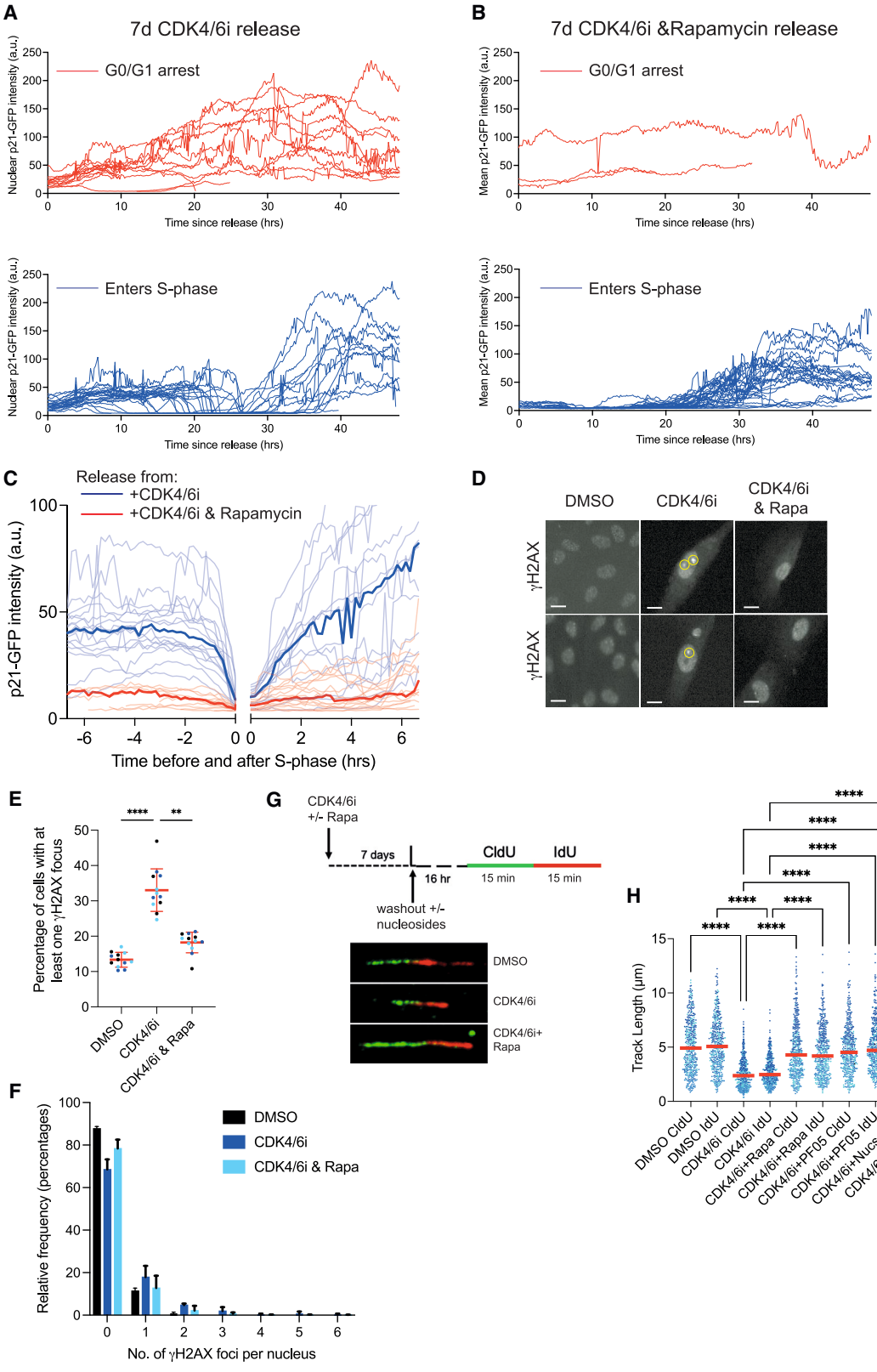

(legend on next page)

upregulating several ROS scavenging and repair pathways, including glutathione biosynthesis and the thioredoxin antioxidant system. NRF2 activity can be increased using the small molecule TBE-31,[42] which stabilizes NRF2 by inhibiting its E3 ligase KEAP1.[43] Treatment with TBE-31 leads to increased expression of the NRF2 target gene NQO1 (Figure S4D) demonstrating NRF2 activation, but fails to prevent p21 induction (Figures S4D and S4E). Therefore, our data suggest that, although CDK4/6i increases ROS,[15,32,33] increased ROS levels do not appear to be critical for p21 induction in RPE1 cells.

Overgrowth has been associated with cytoplasmic dilution,[21] which must be osmoregulated. To investigate if osmotic stress could contribute to p21 induction, we tested whether extracellular osmolyte concentration can modulate p21 levels in CDK4/6i-treated cells. Cells arrested for 1 day in CDK4/6i were cultured for an additional 3 days in CDK4/6i with media with different osmolarities: hypertonic (703 mOsm/kg), hypotonic (179 mOsm/kg), and isotonic (300 mOsm/kg). Critically, nutrient concentrations were identical between media. The only varying component was the concentration of D-sorbitol, either absent (hypotonic), restored to basal levels (isotonic), or present in excess (hypertonic). Addition of hypertonic media to asynchronous cells increases p21 levels, as expected[39] (Figure S4F). However, in CDK4/6i cells, hypertonic media suppresses p21 induction (Figures 4A and 4B). Effects on cell size were negligible or minor (Figure S4G), presumably because of the timescale of treatment with hypertonic media (3 days) and homeostatic regulatory volume increase.[44] In addition to suppressing p21 induction, hypertonic media decreases the frequencies of durable G0/G1 and G2 arrest following drug washout from 4-day (Figure S4H) and 7-day CDK4/6i treatment (Figure 4C).

These data show that altering the osmolarity of extracellular media can limit the induction of p21 expression and cell cycle exit phenotypes following drug washout. Next, we wanted to further investigate the possibility that cell overgrowth may induce, or exacerbate, osmotic stress.

Cell growth during prolonged G0/G1 arrest activates an osmoadaptive response

Osmotic stress occurs when extracellular and intracellular osmolarities differ. In CDK4/6i-treated cells, a change in the osmolarity of the culture media is unlikely. However, it is possible that cell overgrowth challenges osmotic balance by affecting intracellular osmolarity. For example, intracellular osmotic forces play key roles in morphological changes in cells cultured in isotonic media,[45–47] including cell flattening during cell-matrix attachment[45] and cell rounding during mitosis.[46] Cells respond to hyperosmotic stress by regulatory volume increase.[44] Signal transduction and gene expression changes lead to accumulation of intracellular osmolytes,[48] which buffer cells against extracellular hyperosmotic conditions. We predicted that if cells experience osmotic stress in becoming aberrantly large, then we should observe induction of osmotic adaptation pathways.

Osmotic stress activates a signaling pathway involving the stress-associated p38 mitogen-activated protein kinase (p38MAPK, Figure 4D).[49] Many proteins in this pathway were detected in our proteomics dataset and shown to increase during CDK4/6i treatment (Figures 4D–4F). The scaffolding protein OSM (*CCM2*) recruits Rac, MEKK3, and MKK3 to activate p38MAPK. OSM increases by 40- to 60-fold at day 4 and day 7 CDK4/6i (Figure 4E). The levels of total MKK3 and p38MAPK increase (Figures 4E and 4F). To explore this further, we assayed active p38MAPK, by measuring phospho-p38MAPK pT180/pY182 normalizing to Histone H3 (Figure 4E), allowing direct comparison with the proteomic data. Total and phospho-p38 increase in large cells (~7-fold increase at 7 days), and phospho-HSP27, a downstream readout of p38 activity, increases considerably more (23-fold at 7 days), consistent with increased p38MAPK pathway signaling.[50]

p38MAPK activates the transcription factor NFAT5[51] to promote the expression of genes important in osmotic regulation,[48] including aldose reductase (AR), sorbitol dehydrogenase (SORD), and the phospholipase—neuropathy target esterase (PNPLA6), which all increase with cell size (Figure 4E). Size constraining cells by rapamycin treatment largely blunts induction of these osmotic stress response factors (Figure S4I), resulting in no significant change or a decrease in the levels of MKK3, p38MAPKα, OSM, AR, and SORD. An exception is PNPLA6, which increases in rapamycin co-treated cells.

In response to acute osmotic shock, cells rapidly employ regulated volume changes to return to homeostasis, including upregulating small anion and cation transporters.[44] Consistent with an osmoadaptive response, the LRRC8D subunit of the volume regulated anion channel (VRAC),[50] and the potassium chloride

Figure 3. Biphasic accumulation of p21 drives long-term cell cycle arrest from G0/G1 or G2

(A and B) Nuclear p21-GFP intensity measured in RPE1 mRuby-PCNA p21-GFP cells released from 7-day CDK4/6i ([A], n = 44 cells) or CDK4/6i and rapamycin co-treatment ([B], n = 41 cells). Red curves are cells that remain in a G0/G1 arrest, blue curves are cells that enter S-phase.

(C) Same data in Figure 3A showing nuclear p21-GFP intensity in cells released from 7-day CDK4/6i (blue curve) or CDK4/6i and rapamycin co-treatment (red curve). Here, only cells that enter and exit S-phase during the imaging period are shown and data are aligned around S-phase entry and exit (time 0 h). Bold line is median p21-GFP intensity and faint lines are single-cell p21-GFP levels.

(D) Images show representative nuclei stained for γH2AX of the conditions in the graphs in (E) and (F). Yellow circles highlight the large γH2AX foci quantified. Scale bars, 20 μm.

(E and F) Graphs showing quantification of DNA damage foci 48 h after cells are released from a 7-day CDK4/6i or CDK4/6i+rapamycin arrest. Graphs show fraction of nuclei with at least one DNA damage focus marked by γH2AX (E) or the number of large γH2AX foci per nucleus (F). Data are plotted as superplots. Mean ± SD of n = 3 are shown in red.

(G) Schematic of CDK4/6i washout DNA fiber experiments. RPE1 cells were treated with CDK4/6i, or CDK4/6i+rapamycin for 7 days before 16 h washout in drug-free media in the presence or absence of EmbryoMax nucleoside supplementation. Cells were sequentially pulsed with CldU (green) and IdU (red) to label nascent DNA. Representative images of DNA fibers from each condition are shown.

(H) RPE1 cells were treated as in (G). Replication progression for both labels is displayed. n = 3 and data are plotted as superplots. Mean is shown in red. One-way ANOVA used to measure significance throughout, ****$p < 0.0001$, **$p < 0.01$.

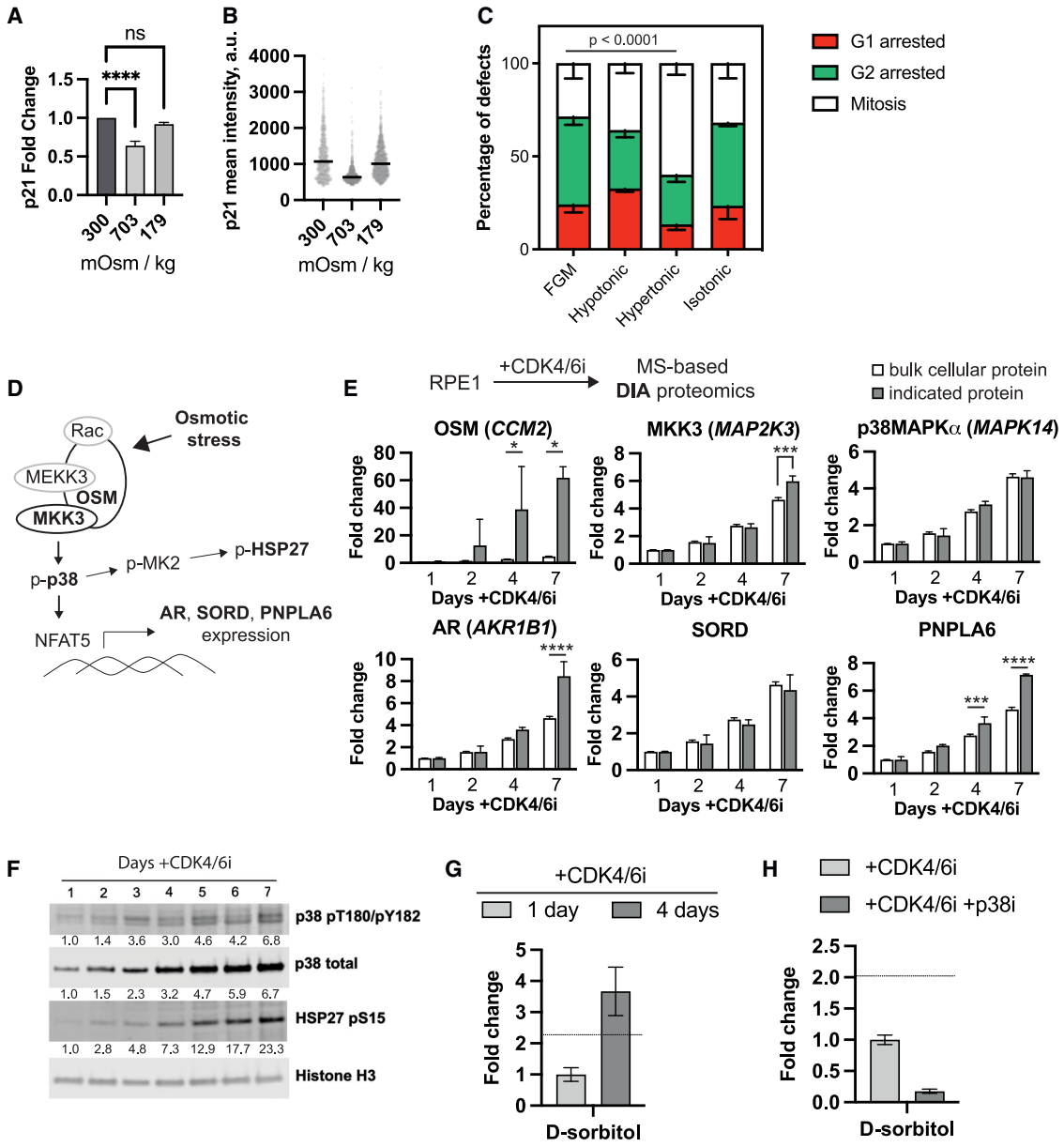

Figure 4. Cell growth during prolonged G0/G1 arrest activates an osmoadaptive response

(A) Flow cytometry analysis of RPE1 cells treated with CDK4/6i for 4 days and either isotonic (300 mOsm/kg), hypertonic (703 mOsm/kg), or hypotonic media (179 mOsm/kg). Cells were immunostained for p21. ****p < 0.0001 from one-way ANOVA with multiple testing correction.

(B) Quantitative immunostaining of RPE1 cells treated as in (A) and immunostained for p21.

(C) The frequency of RPE1 FUCCI cells that remain arrested in G1, enter S-phase and show premature geminin degradation (G2 arrested), or successfully complete mitosis following 7-day CDK4/6i treatment in the respective media types and drug washout. Mean of n = 3 ± SD is shown with 50 cells analyzed per repeat. Mitotic frequencies were compared using a χ^2 test. FGM = full growth media.

(D) An abbreviated schematic of the osmotic shock and osmoadaptation pathway. In bold are proteins identified by proteomics.

(E) Comparison of protein copy fold change of indicated proteins and bulk cellular protein across indicated days of CDK4/6i treatment. Error bars show SEM (n = 2–3). ****, ***, and * indicate p values < 0.0001, < 0.0002, and < 0.03, respectively, from two-way ANOVA with multiple testing correction.

(F) Immunoblot analysis of RPE1 cells treated with CDK4/6i for the indicated days. Densiometric quantitation provided below each band normalized to 1 day (first lane) adjusted for loading using histone H3.

(G) Fold change of D-sorbitol in cells treated with 1- and 4-day CDK4/6i. Assignment confidence is MSI:2 (see STAR Methods).

(H) D-sorbitol levels in RPE1 cells treated with +CDK4/6i vs. +CDK4/6i +p38i for 4 days. Assignment confidence is MSI:2. Dotted lines refer to average increase in metabolites over the 4-day arrest.

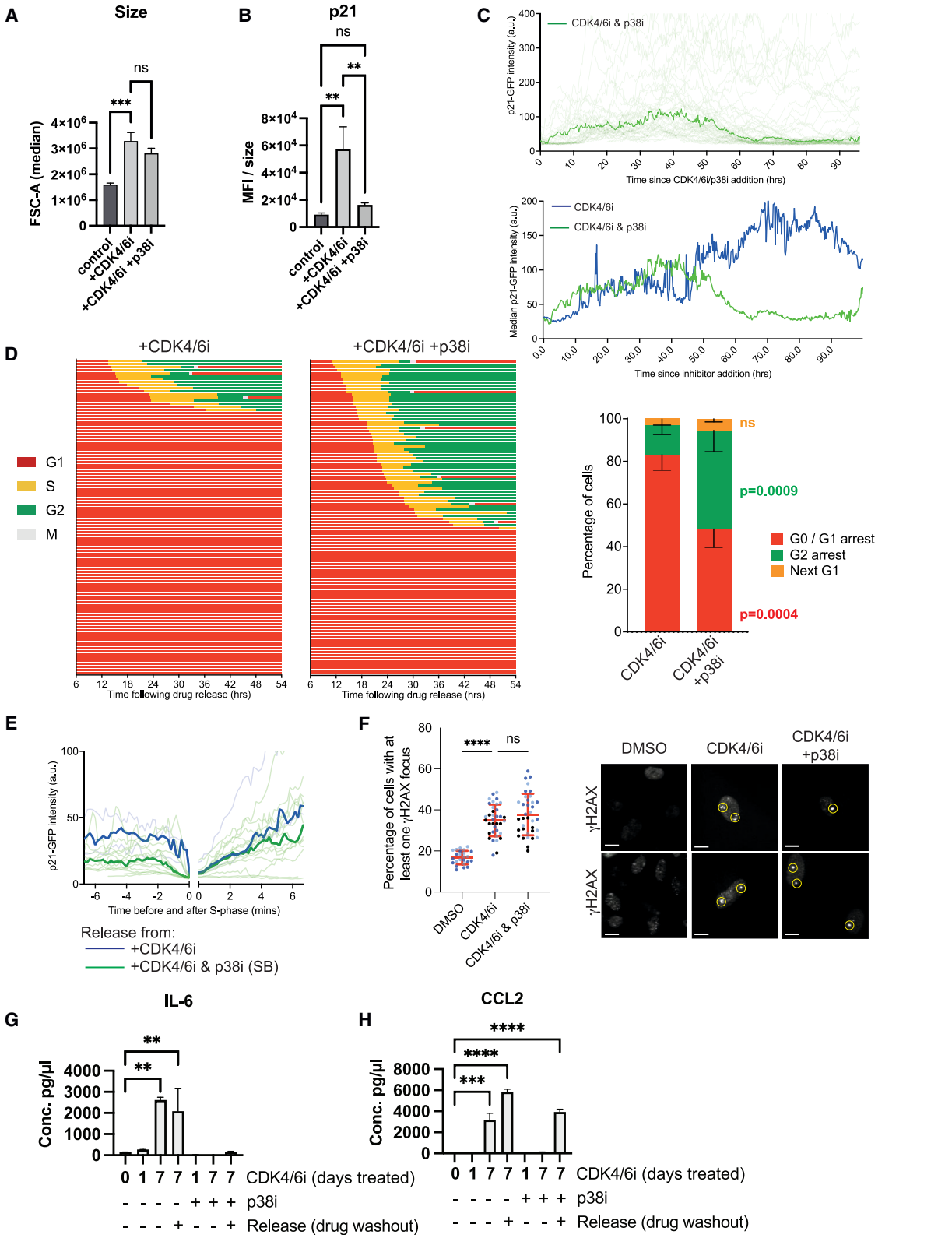

(legend on next page)

exchanger KCC1 that is activated by cell swelling,[52] both increase in cells treated with CDK4/6i (Figure S4J). In summary, we observe growth-dependent increases in proteins involved in osmoregulation, consistent with the idea that overgrowth induces an osmotic stress response.

AR produces sorbitol from glucose and SORD converts sorbitol to fructose, thereby controlling intracellular levels of D-sorbitol, which is critical for osmotic regulation in mammalian cells[48] and retinal cells in particular.[53] To measure levels of D-sorbitol and other metabolites important for intracellular osmolarity regulation, we performed untargeted metabolomics comparing cells treated for 1 and 4 days with CDK4/6i. 416 metabolites were putatively assigned based on accurate mass. Equal numbers of cells from each condition were analyzed. Levels of D-sorbitol increase 3.7-fold in CDK4/6i-treated large cells (Figure 4G), suggesting that the changes in AR and SORD (Figure 4E) produce a net increase in the intracellular concentration of sorbitol. Inhibition of p38 using SB-203580 (p38i[54]) significantly decreases D-sorbitol levels in CDK4/6i-treated cells (Figure 4H), suggesting that p38 activity is important for the observed increase in D-sorbitol. Other osmolytes also increase, including L-carnitine and betaine (Figure S4K). Based on these observations, we conclude that key intracellular osmolytes increase in CDK4/6i-treated cells, consistent with an active osmoadaptive response in overgrown cells.

p38MAPK activity is required for p21 induction during G0/G1 arrest

p38MAPK is a core signaling node downstream of osmotic and other cellular stresses[55] to activate p53 and increase p21.[39] To test if p38MAPK activity plays a role in the first wave of p21 induction, cells were treated with either CDK4/6i alone or combined CDK4/6i and p38i.[54] CDK4/6i and p38i co-treated cells grew to a similar size to CDK4/6i treatment alone (Figures 5A and S5A). p21 induction following CDK4/6i is almost completely prevented by co-treatment with p38i (Figures 5B, S5B, and S5C). Osmotic stress also can activate related stress inducible JNK kinases.[56] However, co-treatment with a small molecule JNK inhibitor (JNK-IN-8), which targets JNK1/2/3, failed to prevent p21 induction (Figure S5D).

To observe at what point during the G0/G1 arrest p38i acts to suppress p21, we used live-cell imaging of RPE1 mRuby-PCNA p21-GFP cells (Figure 5C). As shown before (Figure 2E), p21-GFP levels increase at ~48 h of CDK4/6i treatment. By contrast, p21-GFP induction is not only suppressed in CDK4/6i and p38i co-treated cells but decreases around the same time point (Figure 5C). We conclude that p38MAPK activity is required for p21 induction during a prolonged G0/G1 arrest.

Next, we investigated if suppression of p21 induction by p38i leads to rescue of the long-term cell cycle arrest phenotypes. Co-treatment of RPE1 mRuby-PCNA cells with CDK4/6i and p38i significantly reduced the fraction of cells remaining in a G0/G1 arrest (Figure 5D). A reduction in S-phase entry delay was also observed in RPE1 FUCCI cells and with structurally distinct p38 inhibitors (Figures S5E and S5F).

To understand how CDK4/6i and p38i co-treatment is not able to fully rescue cell cycle withdrawals from G2 (Figures 5D and S5E), we imaged p21-GFP expression in RPE1 mRuby-PCNA p21-GFP after release from 7-day CDK4/6i or CDK4/6i and p38i treatment. As described, p21-GFP levels are lower after washout of CDK4/6i and p38i than of CDK4/6i alone and many more of the co-treated cells re-enter S-phase (blue curves, Figure S5G). However, after completing S-phase, cells released from dual CDK4/6 and p38 inhibition upregulate p21-GFP (Figures 5E and S5G). We also observed increased p21 in fixed cells (Figure S5H). We suspected that this is because CDK4/6i and p38i co-treated cells remain overgrown and may still experience replication stress during the first S-phase after release from CDK4/6i. Therefore, we quantified the level of DNA damage in cells released from CDK4/6i and p38i co-treatment and saw that the levels of DNA damage were equivalent to those in cells treated with CDK4/6i alone (Figure 5F). We also noted that, 48 h after inhibitor washout, CDK4/6i and p38i co-treated cells have similar levels of micronuclei (Figure S5I). This suggests that overgrowth may also be contributing to defects in mitosis, which may contribute to arrest in the next G1.

Durable cell cycle arrest is only one hallmark of cellular senescence.[57,58] Although p38i co-treatment suppresses durable G0/G1 arrest imposed by long-term CDK4/6i, it was unclear if p38i also affects other molecular hallmarks of senescence.

Figure 5. p38MAPK activity is required for p21 induction during G0/G1 arrest and cell cycle defects following release

(A) Forward scatter of cells treated with CDK4/6i or with co-treatment with p38i.

(B) Cells were treated as in (A), immunostained for p21, and assayed by flow cytometry. Median fluorescence intensities (MFI) were normalized to size (forward scatter).

(C) Graph showing nuclear p21-GFP intensity measured in RPE1 mRuby-PCNA p21-GFP H3.1-iRFP cells after addition of CDK4/6i and p38i (SB203580; green curve) or CDK4/6i alone (blue curve) to cells. Median p21-GFP intensity of single-cell data are shown: n = 87 cells for CDK4/6i/p38i (single-cell data shown in faint green curves in top graph).

(D) Graphs show timings of cell cycle phases extracted from time-lapse imaging of RPE1 mRuby-PCNA cells after release from 7-day arrest in CDK4/6i or CDK4/6i+p38i (30 μM SB-203580). In these experiments, cells were released into fresh media with no STLC and therefore were able to complete mitosis and enter the next G1. Accompanying bar chart shows cell fates after release from inhibitors. "Divides" refers to whether cells complete mitosis after release from inhibitors. Mean ± SD of n = 3 are shown. One-way ANOVA was used to measure significance.

(E) Same data in Figure S5G showing nuclear p21-GFP intensity in cells released from 7-day CDK4/6i (blue curve) or CDK4/6i+p38i treatment (green curve). Here, only cells that enter and exit S-phase during the imaging period are shown, and data are aligned around S-phase entry and exit (time 0 h). The line in bold is the median p21-GFP intensity, and the faint lines are single-cell p21-GFP levels.

(F) Graph showing quantification of DNA damage foci 48 h after cells are released from a 7-day CDK4/6i or CDK4/6i+p38i (SB-203580) arrest. Superplot shows fraction of nuclei with at least one γH2A.X large focus. Mean ± SD are shown. One-way ANOVA used to measure significance, ****$p < 0.0001$, ns: not significant. Images show representative nuclei stained for γH2AX in each of the conditions in the graphs. Yellows circles highlight the large γH2AX foci quantified in the graph on the left. Scale bars, 20 μm.

(G and H) Quantitation of IL-6 and CCL2 in conditioned media. One-way ANOVA used to measure significance, ****$p < 0.0001$, ***$p < 0.001$, **$p < 0.01$; n = 2.

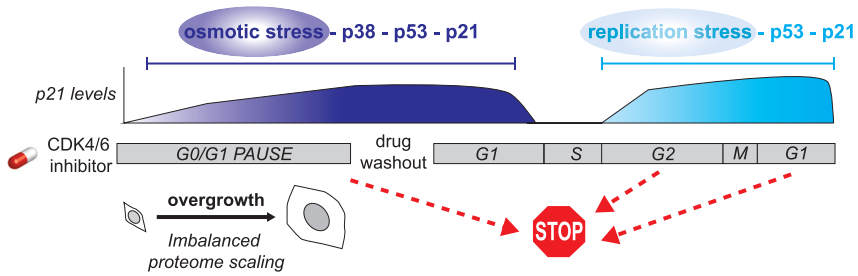

Figure 6. Model for long-term inhibition of proliferation after CDK4/6i removal

Cell overgrowth promotes an osmotic stress response in cells that activates p38MAPK-dependent, p53-dependent p21 expression that leads to permanent cell cycle arrest after CDK4/6i removal. Overgrown cells that re-enter S-phase after CDK4/6i removal experience replication stress, which drives further p21 expression, resulting in permanent G2 arrest or arrest in the subsequent G1.

Treatment with CDK4/6i alone for 7 days increased the fraction of beta-galactosidase (B-gal)-positive cells, and this was significantly reduced in the absence of p21 (Figure S5J). Co-treatment with p38i reduced the fraction of B-gal-positive cells, although this difference was not statistically significant.

Another key hallmark of senescence is the senescence-associated secretory (SASP) phenotype. Long-term treatment with CDK4/6i significantly increases secretion of the pro-inflammatory cytokine IL-6 (Figure 5G). High IL-6 production continues when cells are released from CDK4/6i and enter durable cell cycle arrest. Co-treatment with p38i abolishes IL-6 production (Figure 5G). The chemokine CCL2 is also upregulated following long-term treatment with CDK4/6i (Figure 5H), and this is further increased following release from CDK4/6i. CCL2 is suppressed by p38i co-treatment during CDK4/6i-mediated arrest, but unlike IL-6, is upregulated following drug washout.

Our data show that p38MAPK inhibition can prevent the first wave of p21 expression and secretion of SASP components caused by prolonged CDK4/6i treatment. However, because cells are still aberrantly large, the second wave of p21 expression, which coincides with replication stress, persists; therefore, cells treated with combined CDK4/6i and p38i withdraw from the cell cycle in G2 or the subsequent G1.

DISCUSSION

Cell growth and proliferation are coupled to regulate cell size. Uncoupling these processes has major, negative consequences to cells,[21,22,59,60] but how this uncoupling is transduced at a molecular level remains under investigation. We have shown that cellular overgrowth during prolonged CDK4/6 inhibition promotes long-term cell cycle arrest, even following drug washout. Long-term cell cycle arrest is dependent on p53-dependent p21 protein expression. p21 expression manifests as two waves driven by at least two distinct cellular stresses (Figure 6). The first p21 wave occurs during CDK4/6i treatment, during which osmotic stress promotes p21 expression via p38MAPK. The second p21 wave occurs after removal of CDK4/6i in a fraction of cells that re-enter S-phase. In these cells, aberrant size generates replication stress, which promotes additional p21 expression after S-phase, causing cells to withdraw from the cell cycle in G2 or the next G1. The levels of p21 therefore integrate signals over multiple days from osmotic and replication stress to determine cell fate. Our data thus provide one potential mechanism for the prior observations that CDK4/6i can promote senescence both *in vitro* and *in vivo*.[18,19,21,22,24]

The cytoplasmic dilution model[21] proposes that aberrantly large cells face a fitness penalty due to inefficiencies in gene expression and biochemical reactions in a dilute cytoplasm. A reduction in large macromolecular crowding in an expanding cytoplasmic volume must be accompanied by an increase in more freely diffusing solutes to maintain osmotic balance. We demonstrated that large cells showed activation of an osmolyte biosynthesis pathway via p38, leading to an increase in the intracellular osmolyte sorbitol in cells. Here, p38 activation both regulates intracellular osmolyte concentration and stress signal transduction via p53.

Studies thus far have not demonstrated why osmotic stress and cytoplasmic dilution occur in large cells. We favor the possibility that widespread proteome remodeling (Figure S6A)[60] and loss of proteostasis as one source of osmotic stress. Indeed, unequal gene dosage perturbs protein complex subunit expression and stoichiometry, leading to hypo-osmotic stress.[61] Subunit stoichiometry uncoupling has also been implicated in cellular aging in yeast.[62] However, this model requires robust evaluation and testing.

How factors scale with total protein during overgrowth will clearly impact on their downstream function. However, it is important to point out that even for factors that maintain their normal concentrations during growth, their functions can still be perturbed for other reasons. For example, their downstream substrates may scale differently. This is likely to be crucial for p21 because the downstream substrates that it inhibits, including CDK1 and CDK2, become significantly diluted during cell overgrowth (Figure 2C). Therefore, effective p21:CDK ratios increase, likely contributing to the cell cycle arrest. In addition, subcellular compartments do not uniformly scale proportionally with total protein content (Figure S6A),[60] which makes interpretation of scaling based on biochemical measurements from total cell extracts challenging. This is apparent for the nucleus which subscales with respect to cell volume (Figures 1B, 1F, and S1B), and this may explain why p21 concentration appears to increase in the nucleus by immunofluorescence, although total p21 concentration remains similar by western in large and small cells (Figure S2A). p21 is unlikely the only nuclear protein affected, and, indeed, this broader phenomenon could contribute to replication defects[24] (Figure 3H) or defective DNA damage repair observed in large cells.[35] Unequal scaling of proteins that function by stoichiometric binding, for example scaffolding factors, may also help to explain why p38 concentrations remain similar during growth, although downstream p38 activity, based on HSP27 phosphorylation, appears hyperactivated in overgrown cells (Figure 4F). It will be important to consider these issues in

future when investigating how molecular pathways are perturbed by cellular enlargement.

CDK4/6 and p38MAPK have previously been implicated in the regulation of cell size.[20] There, partial inhibition of CDK4/6 activity during G1 leads to a larger target size for the cell by increasing both the duration and the rate of growth. p38MAPK then acts downstream of changes in cell size, whereby p38 activity increases in cells below their target size and prevents cell cycle progression. The sensor(s) that detect changes in cell size and lead to p38 activation remain unknown. How the p38 pathway is activated downstream of cell overgrowth and osmotic stress will be important to ascertain in future. It is possible that partial inhibition of CDK4/6 activity in proliferating G1 cells by Tan et al.[20] also induces a level of osmotic stress and thereby activates p38.

Cell overgrowth is a secondary effect of inhibiting cell proliferation, and not a direct consequence of CDK4/6i (Figure S6B). By extension, any inhibitors that block cell cycle entry could also lead to cell overgrowth. Recent work has shown that inhibition of CDK7, part of the CDK-activating kinase complex, also arrests cells in G0/G1 and leads to mTOR-dependent cell overgrowth that contributes to long-term cell cycle arrest.[63] Similar effects are observed by CDK2/4/6 inhibition in cell lines that respond poorly to CDK4/6 inhibition alone.[26] Therefore, any perturbations that block the G1/S transition could also cause cell cycle arrest due to overgrowth. This could represent a new paradigm for achieving tumor-specific senescence with general cell cycle drugs, especially because the extent of overgrowth is elevated by oncogenic signals in cancer cells.[26]

It is clear from our data that the increase in replication stress observed in the first S-phase after removal of CDK4/6 inhibition[24] is at least partly due to aberrant cell size. Increased replication stress after CDK4/6i removal has been attributed to decreased concentrations of proteins involved in DNA replication origin licensing and DNA replication.[24] We observe altered replication dynamics following successful origin firing, demonstrating here that aberrantly large cells display decreased replication fork progression, which is restored by constraining cell size. Furthermore, the Neurohr lab observed that larger cells are less efficient at repairing DNA damage.[35] Therefore, the combination of increased replication stress-induced DNA damage and inefficient DNA damage repair both likely contribute to the problems experienced by overgrown cells during S-phase.

Replication fork progression was also restored by nucleoside supplementation. The underlying mechanisms are yet to be determined, although we hypothesize that nucleotide levels may become limiting in enlarged cells that must upregulate mRNA and ribosome production. However, we must also acknowledge that the broader mechanisms via which nucleoside supplementation has previously been demonstrated to ameliorate replication stress-induced genome instability are poorly understood.[64,65] We also cannot rule out the possibility that changes in chromatin organization during CDK4/6i treatment and/or cell overgrowth may contribute to replication stress, and this remains to be explored.

Our data have consequences for the use CDK4/6i in the clinic. For example, 60% of CDK4/6i-resistant breast cancer patients have mutations in TP53.[12] The authors found that p53 knockout cells still arrested in CDK4/6i and therefore were unable to explain mutant p53's contributions to therapy resistance, despite the fact that p53 mutations had also been associated with resistance in a previous study.[66] We also observed that neither p53 or p21 are required for cells to arrest in G0/G1 with CDK4/6i.[24,26,30] However, the data presented here, and that of others,[18,24,26] show that a functional p53-p21 pathway is required after CDK4/6i removal to mediate long-term cell cycle arrest. Indeed, recent data suggest that p21 promotes long-term responses in breast cancer cells by inhibiting phosphorylation of p130 by CDK2.[67]

Finally, p53 loss is predicted to confer more resistance than p38 loss because it also antagonizes the replication-stress-induced DNA damage response. Because the secretory phenotype of senescent cells varies depending on DNA damage,[18] the lack of DNA damage in p38-dependent long-term cell cycle arrest suggests that modulating p38 activity in combination with CDK4/6 inhibition could result in a clinically beneficial secretory phenotype by promoting immunosurveillance without pro-proliferative and pro-migratory paracrine signaling to neighboring tumor cells. Indeed, p38 activity is sufficient for SASP independent of DNA damage signaling.[68] Cell overgrowth, in activating p38, could promote two hallmark characteristics of senescence: permanent cell cycle arrest via p53 and an inflammatory secretory phenotype.

Limitations of the study

The overgrowth stress mechanisms have been studied in a non-transformed, immortalized RPE1 epithelial cell line and the MCF7 cell line, derived from ER+ breast cancer and therefore clinically relevant for CDK4/6i therapy. Future work will need to investigate these mechanisms in 3D organoids, *in vivo* models, and clinical samples, where tumor microenvironment, genetic mutations, and multi-morbidities may impact on the levels of osmotic or replication stress. A crucial question will be to determine whether overgrowth, osmotic stress, p21 induction, and DNA damage are observed prior to senescence.

Osmoadaptive stress and replication stress occur at distinct time windows (G0/G1 arrest and cell cycle re-entry, respectively) and our study does not address if the former can directly impact the latter. Cells with the highest levels of p21 during G0/G1 arrest fail to re-enter the cell cycle, suggesting that osmoadaptive stress prevents replication stress. It is possible that intermediate levels of osmoadaptive stress can enhance replication stress, with p53 activity acting as a stress integrator, as previously suggested in other contexts.[69] It will be important to test this model robustly and to investigate potential direct mechanistic links between osmotic and replication stress.

STAR★METHODS

Detailed methods are provided in the online version of this paper and include the following:

- KEY RESOURCES TABLE
- RESOURCE AVAILABILITY

SUPPLEMENTAL INFORMATION

Supplemental information can be found online at https://doi.org/10.1016/j.molcel.2023.10.016.

ACKNOWLEDGMENTS

We thank colleagues in the Ly, Saurin, and Barr groups for helpful discussions. We thank Edward Kaye (Dundee), Christos Spanos and Van Kelly (Wellcome Centre for Cell Biology), and Alex Montoya and Holger Kramer (MRC-LMS proteomics core) for help with mass spectrometry analysis. This work was supported by a Cancer Research UK Programme Foundation Award to A.T.S. (C47320/A21229), which also funds L.C. and R.F.; a Tenovus Scotland Studentship (which funded R.F.); a Medical Research Council (UK) Doctoral Training Program Studentship (which funded L.C.); a Ninewells Cancer Campaign studentship (which funds A.U.P.), a Wellcome Trust Investigator Award to A.T.S. (222494/Z/21/Z), which also funds J.M.V., a Wellcome-Royal Society Sir Henry Dale Fellowship to T.L. (206211/A/17/Z, 218305/Z/19/Z), a CRUK Career Development Fellowship to A.R.B. (C63833/A25729), and MRC-LMS core funding to A.R.B. to support R.A., J.A.H., and W.A.W. (MC-A658-5TY60).

AUTHOR CONTRIBUTIONS

A.T.S., A.R.B., and T.L. conceived the study. A.T.S., A.R.B., T.L., L.C., R.F., and R.A. designed experiments. A.R.B., T.L., L.C., R.F., R.A., and all remaining authors conducted and analyzed experiments. P.W. and C.R. performed the metabolomics analysis. L.G.B., E.G.V., A.G., and C.J.S. performed and analyzed the replication fork speed experiments. A.T.S., A.R.B., and T.L. wrote the manuscript.

DECLARATION OF INTERESTS

The authors declare no competing interests.

Received: September 12, 2022
Revised: July 10, 2023
Accepted: October 16, 2023
Published: November 16, 2023

REFERENCES

1. Cristofanilli, M., Turner, N.C., Bondarenko, I., Ro, J., Im, S.A., Masuda, N., Colleoni, M., DeMichele, A., Loi, S., Verma, S., et al. (2016). Fulvestrant plus palbociclib versus fulvestrant plus placebo for treatment of hormone-receptor-positive, HER2-negative metastatic breast cancer that progressed on previous endocrine therapy (PALOMA-3): final analysis of the multicentre, double-blind, phase 3 randomised controlled trial. Lancet Oncol. *17*, 425–439. https://doi.org/10.1016/S1470-2045(15)00613-0.
2. Im, S.A., Lu, Y.S., Bardia, A., Harbeck, N., Colleoni, M., Franke, F., Chow, L., Sohn, J., Lee, K.S., Campos-Gomez, S., et al. (2019). Overall survival with Ribociclib plus endocrine therapy in breast cancer. N. Engl. J. Med. *381*, 307–316. https://doi.org/10.1056/NEJMoa1903765.
3. Dickler, M.N., Tolaney, S.M., Rugo, H.S., Cortés, J., Diéras, V., Patt, D., Wildiers, H., Hudis, C.A., O'Shaughnessy, J., Zamora, E., et al. (2017). MONARCH 1, A Phase II study of Abemaciclib, a CDK4 and CDK6 inhibitor, as a single agent, in patients with refractory HR+/HER2− metastatic breast cancer. Clin. Cancer Res. *23*, 5218–5224. https://doi.org/10.1158/1078-0432.CCR-17-0754.
4. Álvarez-Fernández, M., and Malumbres, M. (2020). Mechanisms of sensitivity and resistance to CDK4/6 inhibition. Cancer Cell *37*, 514–529. https://doi.org/10.1016/j.ccell.2020.03.010.
5. Matthews, H.K., Bertoli, C., and de Bruin, R.A.M. (2022). Cell cycle control in cancer. Nat. Rev. Mol. Cell Biol. *23*, 74–88. https://doi.org/10.1038/s41580-021-00404-3.
6. Matsushime, H., Ewen, M.E., Strom, D.K., Kato, J.Y., Hanks, S.K., Roussel, M.F., and Sherr, C.J. (1992). Identification and properties of an atypical catalytic subunit (p34PSK-J3/cdk4) for mammalian D type G1 cyclins. Cell *71*, 323–334. https://doi.org/10.1016/0092-8674(92)90360-O.
7. Sherr, C.J. (1993). Mammalian G1 cyclins. Cell *73*, 1059–1065. https://doi.org/10.1016/0092-8674(93)90636-5.
8. Knudsen, E.S., and Witkiewicz, A.K. (2017). The strange case of CDK4/6 inhibitors: mechanisms, resistance, and combination strategies. Trends Cancer *3*, 39–55. https://doi.org/10.1016/j.trecan.2016.11.006.
9. Fassl, A., Geng, Y., and Sicinski, P. (2022). CDK4 and CDK6 kinases: from basic science to cancer therapy. Science *375*, eabc1495. https://doi.org/10.1126/science.abc1495.
10. Goel, S., Bergholz, J.S., and Zhao, J.J. (2022). Targeting CDK4 and CDK6 in cancer. Nat. Rev. Cancer *22*, 356–372. https://doi.org/10.1038/s41568-022-00456-3.
11. Klein, M.E., Kovatcheva, M., Davis, L.E., Tap, W.D., and Koff, A. (2018). CDK4/6 inhibitors: the mechanism of action may not be as simple as once thought. Cancer Cell *34*, 9–20. https://doi.org/10.1016/j.ccell.2018.03.023.
12. Wander, S.A., Cohen, O., Gong, X., Johnson, G.N., Buendia-Buendia, J.E., Lloyd, M.R., Kim, D., Luo, F., Mao, P., Helvie, K., et al. (2020). The genomic landscape of intrinsic and acquired resistance to cyclin-dependent kinase 4/6 inhibitors in patients with hormone receptor–positive metastatic breast cancer. Cancer Discov. *10*, 1174–1193. https://doi.org/10.1158/2159-8290.CD-19-1390.
13. Gong, X., Litchfield, L.M., Webster, Y., Chio, L.C., Wong, S.S., Stewart, T.R., Dowless, M., Dempsey, J., Zeng, Y., Torres, R., et al. (2017). Genomic aberrations that activate D-type cyclins are associated with enhanced sensitivity to the CDK4 and CDK6 inhibitor Abemaciclib. Cancer Cell *32*, 761–776.e6. https://doi.org/10.1016/j.ccell.2017.11.006.
14. Deng, J., Wang, E.S., Jenkins, R.W., Li, S., Dries, R., Yates, K., Chhabra, S., Huang, W., Liu, H., Aref, A.R., et al. (2018). CDK4/6 inhibition augments antitumor immunity by enhancing T-cell activation. Cancer Discov. *8*, 216–233. https://doi.org/10.1158/2159-8290.CD-17-0915.
15. Goel, S., DeCristo, M.J., Watt, A.C., BrinJones, H., Sceneay, J., Li, B.B., Khan, N., Ubellacker, J.M., Xie, S., Metzger-Filho, O., et al. (2017). CDK4/6 inhibition triggers anti-tumour immunity. Nature *548*, 471–475. https://doi.org/10.1038/nature23465.

16. Lelliott, E.J., Kong, I.Y., Zethoven, M., Ramsbottom, K.M., Martelotto, L.G., Meyran, D., Zhu, J.J., Costacurta, M., Kirby, L., Sandow, J.J., et al. (2021). CDK4/6 inhibition promotes antitumor immunity through the induction of T-cell memory. Cancer Discov. *11*, 2582–2601. https://doi.org/10.1158/2159-8290.CD-20-1554.

17. Heckler, M., Ali, L.R., Clancy-Thompson, E., Qiang, L., Ventre, K.S., Lenehan, P., Roehle, K., Luoma, A., Boelaars, K., Peters, V., et al. (2021). Inhibition of cdk4/6 promotes CD8 T-cell memory formation. Cancer Discov. *11*, 2564–2581. https://doi.org/10.1158/2159-8290.CD-20-1540.

18. Wang, B., Varela-Eirin, M., Brandenburg, S.M., Hernandez-Segura, A., van Vliet, T., Jongbloed, E.M., Wilting, S.M., Ohtani, N., Jager, A., and Demaria, M. (2022). Pharmacological CDK4/6 inhibition reveals a p53-dependent senescent state with restricted toxicity. EMBO J. *41*, e108946. https://doi.org/10.15252/embj.2021108946.

19. Wagner, V., and Gil, J. (2020). Senescence as a therapeutically relevant response to CDK4/6 inhibitors. Oncogene *39*, 5165–5176. https://doi.org/10.1038/s41388-020-1354-9.

20. Tan, C., Ginzberg, M.B., Webster, R., Iyengar, S., Liu, S., Papadopoli, D., Concannon, J., Wang, Y., Auld, D.S., Jenkins, J.L., et al. (2021). Cell size homeostasis is maintained by CDK4-dependent activation of p38 MAPK. Dev. Cell *56*, 1756–1769.e7. https://doi.org/10.1016/j.devcel.2021.04.030.

21. Neurohr, G.E., Terry, R.L., Lengefeld, J., Bonney, M., Brittingham, G.P., Moretto, F., Miettinen, T.P., Vaites, L.P., Soares, L.M., Paulo, J.A., et al. (2019). Excessive cell growth causes cytoplasm dilution and contributes to senescence. Cell *176*, 1083–1097.e18. https://doi.org/10.1016/j.cell.2019.01.018.

22. Lengefeld, J., Cheng, C.W., Maretich, P., Blair, M., Hagen, H., McReynolds, M.R., Sullivan, E., Majors, K., Roberts, C., Kang, J.H., et al. (2021). Cell size is a determinant of stem cell potential during aging. Sci. Adv. *7*, eabk0271. https://doi.org/10.1126/sciadv.abk0271.

23. Korotchkina, L.G., Leontieva, O.V., Bukreeva, E.I., Demidenko, Z.N., Gudkov, A.V., and Blagosklonny, M.V. (2010). The choice between p53-induced senescence and quiescence is determined in part by the mTOR pathway. Aging *2*, 344–352. https://doi.org/10.18632/aging.100160.

24. Crozier, L., Foy, R., Mouery, B.L., Whitaker, R.H., Corno, A., Spanos, C., Ly, T., Gowen Cook, J.G., and Saurin, A.T. (2022). CDK4/6 inhibitors induce replication stress to cause long-term cell cycle withdrawal. EMBO J. *41*, e108599. https://doi.org/10.15252/embj.2021108599.

25. Barr, A.R., and McClelland, S.E. (2022). Cells on lockdown: long-term consequences of CDK4/6 inhibition. EMBO J. *41*, e110764. https://doi.org/10.15252/embj.2022110764.

26. Foy, R., Crozier, L., Pareri, A.U., Valverde, J.M., Park, B.H., Ly, T., and Saurin, A.T. (2023). Oncogenic signals prime cancer cells for toxic cell overgrowth during a G1 cell cycle arrest. Mol. Cell *83*. https://doi.org/10.1101/2022.09.08.506962.

27. Trotter, E.W., and Hagan, I.M. (2020). Release from cell cycle arrest with Cdk4/6 inhibitors generates highly synchronized cell cycle progression in human cell culture. Open Biol. *10*, 200200. https://doi.org/10.1098/rsob.200200.

28. Krenning, L., Feringa, F.M., Shaltiel, I.A., van den Berg, J., and Medema, R.H. (2014). Transient activation of p53 in G2 phase is sufficient to induce senescence. Mol. Cell *55*, 59–72. https://doi.org/10.1016/j.molcel.2014.05.007.

29. Sakaue-Sawano, A., Kurokawa, H., Morimura, T., Hanyu, A., Hama, H., Osawa, H., Kashiwagi, S., Fukami, K., Miyata, T., Miyoshi, H., et al. (2008). Visualizing Spatiotemporal Dynamics of Multicellular Cell-Cycle Progression. Cell *132*, 487–498. https://doi.org/10.1016/j.cell.2007.12.033.

30. Pennycook, B.R., and Barr, A.R. (2021). Palbociclib-mediated cell cycle arrest can occur in the absence of the CDK inhibitors p21 and p27. Open Biol. *11*, 210125. https://doi.org/10.1098/rsob.210125.

31. Barr, A.R., Cooper, S., Heldt, F.S., Butera, F., Stoy, H., Mansfeld, J., Novák, B., and Bakal, C. (2017). DNA damage during S-phase mediates the proliferation-quiescence decision in the subsequent G1 via p21 expression. Nat. Commun. *8*, 14728. https://doi.org/10.1038/ncomms14728.

32. Zerjatke, T., Gak, I.A., Kirova, D., Fuhrmann, M., Daniel, K., Gonciarz, M., Müller, D., Glauche, I., and Mansfeld, J. (2017). Quantitative cell cycle analysis based on an endogenous all-in-one reporter for cell tracking and classification. Cell Rep. *19*, 1953–1966. https://doi.org/10.1016/j.celrep.2017.05.022.

33. Abbas, T., Sivaprasad, U., Terai, K., Amador, V., Pagano, M., and Dutta, A. (2008). PCNA-dependent regulation of p21 ubiquitylation and degradation via the CRL4Cdt2 ubiquitin ligase complex. Genes Dev. *22*, 2496–2506. https://doi.org/10.1101/gad.1676108.

34. Nishitani, H., Shiomi, Y., Iida, H., Michishita, M., Takami, T., and Tsurimoto, T. (2008). CDK inhibitor p21 is degraded by a proliferating cell nuclear antigen-coupled Cul4-DDB1^{Cdt2} pathway during S phase and after UV irradiation. J. Biol. Chem. *283*, 29045–29052. https://doi.org/10.1074/jbc.M806045200.

35. Manohar, S., Estrada, M.E., Uliana, F., Vuina, K., Moyano Alvarez, P., de Bruin, R.A.M., and Neurohr, G.E. (2023). Genome homeostasis defects drive enlarged cells into senescence. Mol. Cell *83*. https://doi.org/10.1101/2022.09.08.506740.

36. El-Deiry, W.S., Harper, J.W., O'Connor, P.M., Velculescu, V.E., Canman, C.E., Jackman, J., Pietenpol, J.A., Burrell, M., Hill, D.E., and Wang, Y. (1994). WAF1/CIP1 is induced in p53-mediated G1 arrest and Apoptosis1. Cancer Res. *54*, 1169–1174.

37. Dulić, V., Kaufmann, W.K., Wilson, S.J., Tlsty, T.D., Lees, E., Harper, J.W., Elledge, S.J., and Reed, S.I. (1994). p53-dependent inhibition of cyclin-dependent kinase activities in human fibroblasts during radiation-induced G1 arrest. Cell *76*, 1013–1023. https://doi.org/10.1016/0092-8674(94)90379-4.

38. Barnouin, K., Dubuisson, M.L., Child, E.S., Fernandez de Mattos, S., Glassford, J., Medema, R.H., Mann, D.J., and Lam, E.W.-F. (2002). H2O2 induces a transient multi-phase cell cycle arrest in mouse fibroblasts through modulating cyclin D and p21Cip1 expression. J. Biol. Chem. *277*, 13761–13770. https://doi.org/10.1074/jbc.M111123200.

39. Kishi, H., Nakagawa, K., Matsumoto, M., Suga, M., Ando, M., Taya, Y., and Yamaizumi, M. (2001). Osmotic shock induces G1 arrest through p53 phosphorylation at Ser33 by activated p38MAPK without phosphorylation at Ser15 and Ser20. J. Biol. Chem. *276*, 39115–39122. https://doi.org/10.1074/jbc.M105134200.

40. Franco, J., Balaji, U., Freinkman, E., Witkiewicz, A.K., and Knudsen, E.S. (2016). Metabolic reprogramming of pancreatic cancer mediated by CDK4/6 inhibition elicits unique vulnerabilities. Cell Rep. *14*, 979–990. https://doi.org/10.1016/j.celrep.2015.12.094.

41. Tonelli, C., Chio, I.I.C., and Tuveson, D.A. (2018). Transcriptional regulation by Nrf2. Antioxid. Redox Signal. *29*, 1727–1745. https://doi.org/10.1089/ars.2017.7342.

42. Dinkova-Kostova, A.T., Talalay, P., Sharkey, J., Zhang, Y., Holtzclaw, W.D., Wang, X.J., David, E., Schiavoni, K.H., Finlayson, S., Mierke, D.F., et al. (2010). An exceptionally potent inducer of cytoprotective enzymes: elucidation of the structural features that determine inducer potency and reactivity with Keap1. J. Biol. Chem. *285*, 33747–33755. https://doi.org/10.1074/jbc.M110.163485.

43. Dinkova-Kostova, A.T., Holtzclaw, W.D., Cole, R.N., Itoh, K., Wakabayashi, N., Katoh, Y., Yamamoto, M., and Talalay, P. (2002). Direct evidence that sulfhydryl groups of Keap1 are the sensors regulating induction of phase 2 enzymes that protect against carcinogens and oxidants. Proc. Natl. Acad. Sci. USA *99*, 11908–11913. https://doi.org/10.1073/pnas.172398899.

44. Hoffmann, E.K., Lambert, I.H., and Pedersen, S.F. (2009). Physiology of cell volume regulation in vertebrates. Physiol. Rev. *89*, 193–277. https://doi.org/10.1152/physrev.00037.2007.

45. Venkova, L., Vishen, A.S., Lembo, S., Srivastava, N., Duchamp, B., Ruppel, A., Williart, A., Vassilopoulos, S., Deslys, A., Garcia Arcos, J.M., et al. (2022). A mechano-osmotic feedback couples cell volume to the rate of cell deformation. eLife *11*, e72381. https://doi.org/10.7554/eLife.72381.

46. Stewart, M.P., Helenius, J., Toyoda, Y., Ramanathan, S.P., Muller, D.J., and Hyman, A.A. (2011). Hydrostatic pressure and the actomyosin cortex drive mitotic cell rounding. Nature *469*, 226–230. https://doi.org/10.1038/nature09642.

47. Stangherlin, A., Watson, J.L., Wong, D.C.S., Barbiero, S., Zeng, A., Seinkmane, E., Chew, S.P., Beale, A.D., Hayter, E.A., Guna, A., et al. (2021). Compensatory ion transport buffers daily protein rhythms to regulate osmotic balance and cellular physiology. Nat. Commun. *12*, 6035. https://doi.org/10.1038/s41467-021-25942-4.

48. Burg, M.B., and Ferraris, J.D. (2008). Intracellular organic osmolytes: function and regulation. J. Biol. Chem. *283*, 7309–7313. https://doi.org/10.1074/jbc.R700042200.

49. Uhlik, M.T., Abell, A.N., Johnson, N.L., Sun, W., Cuevas, B.D., Lobel-Rice, K.E., Horne, E.A., Dell'Acqua, M.L., and Johnson, G.L. (2003). Rac-MEKK3-MKK3 scaffolding for p38 MAPK activation during hyperosmotic shock. Nat. Cell Biol. *5*, 1104–1110. https://doi.org/10.1038/ncb1071.

50. Voss, F.K., Ullrich, F., Münch, J., Lazarow, K., Lutter, D., Mah, N., Andrade-Navarro, M.A., von Kries, J.P., Stauber, T., and Jentsch, T.J. (2014). Identification of LRRC8 heteromers as an essential component of the volume-regulated anion channel VRAC. Science *344*, 634–638. https://doi.org/10.1126/science.1252826.

51. Ko, B.C.B., Lam, A.K.M., Kapus, A., Fan, L., Chung, S.K., and Chung, S.S.M. (2002). Fyn and p38 signaling are both required for maximal hypertonic activation of the osmotic response element-binding protein/tonicity-responsive enhancer-binding protein (OREBP/TonEBP). J. Biol. Chem. *277*, 46085–46092. https://doi.org/10.1074/jbc.M208138200.

52. Mercado, A., Song, L., Vázquez, N., Mount, D.B., and Gamba, G. (2000). Functional comparison of the K+-Cl−Cotransporters KCC1 and KCC4. J. Biol. Chem. *275*, 30326–30334. https://doi.org/10.1074/jbc.M003112200.

53. Lightman, S. (1993). Does aldose reductase have a role in the development of the ocular complications of diabetes? Eye (Lond) *7*, 238–241. https://doi.org/10.1038/eye.1993.56.

54. Cuenda, A., Rouse, J., Doza, Y.N., Meier, R., Cohen, P., Gallagher, T.F., Young, P.R., and Lee, J.C. (1995). SB 203580 is a specific inhibitor of a MAP kinase homologue which is stimulated by cellular stresses and interleukin-1. FEBS Lett *364*, 229–233. https://doi.org/10.1016/0014-5793(95)00357-F.

55. Cuenda, A., and Rousseau, S. (2007). p38 MAP-Kinases pathway regulation, function and role in human diseases. Biochim. Biophys. Acta *1773*, 1358–1375. https://doi.org/10.1016/j.bbamcr.2007.03.010.

56. Galcheva-Gargova, Z., Dérijard, B., Wu, I.H., and Davis, R.J. (1994). An osmosensing signal transduction pathway in mammalian cells. Science *265*, 806–808. https://doi.org/10.1126/science.8047888.

57. Kohli, J., Wang, B., Brandenburg, S.M., Basisty, N., Evangelou, K., Varela-Eirin, M., Campisi, J., Schilling, B., Gorgoulis, V., and Demaria, M. (2021). Algorithmic assessment of cellular senescence in experimental and clinical specimens. Nat. Protoc. *16*, 2471–2498. https://doi.org/10.1038/s41596-021-00505-5.

58. Gorgoulis, V., Adams, P.D., Alimonti, A., Bennett, D.C., Bischof, O., Bishop, C., Campisi, J., Collado, M., Evangelou, K., Ferbeyre, G., et al. (2019). Cellular senescence: defining a path forward. Cell *179*, 813–827. https://doi.org/10.1016/j.cell.2019.10.005.

59. Cheng, L., Chen, J., Kong, Y., Tan, C., Kafri, R., and Björklund, M. (2021). Size-scaling promotes senescence-like changes in proteome and organelle content. Preprint at bioRxiv. https://doi.org/10.1101/2021.08.05.455193.

60. Lanz, M.C., Zatulovskiy, E., Swaffer, M.P., Zhang, L., Ilerten, I., Zhang, S., You, D.S., Marinov, G., McAlpine, P., Elias, J.E., et al. (2022). Increasing cell size remodels the proteome and promotes senescence. Mol. Cell *82*, 3255–3269.e8. https://doi.org/10.1016/j.molcel.2022.07.017.

61. Tsai, H.J., Nelliat, A.R., Choudhury, M.I., Kucharavy, A., Bradford, W.D., Cook, M.E., Kim, J., Mair, D.B., Sun, S.X., Schatz, M.C., et al. (2019). Hypo-osmotic-like stress underlies general cellular defects of aneuploidy. Nature *570*, 117–121. https://doi.org/10.1038/s41586-019-1187-2.

62. Janssens, G.E., Meinema, A.C., González, J., Wolters, J.C., Schmidt, A., Guryev, V., Bischoff, R., Wit, E.C., Veenhoff, L.M., and Heinemann, M. (2015). Protein biogenesis machinery is a driver of replicative aging in yeast. eLife *4*, e08527. https://doi.org/10.7554/eLife.08527.

63. Wilson, G.A., Vuina, K., Sava, G., Huard, C., Meneguello, L., Coulombe-Huntington, J., Bertomeu, T., Maizels, R.J., Lauring, J., Kriston-Visi, J., et al. (2021). Active growth signaling promotes senescence and cancer cell sensitivity to CDK7 inhibition. Mol. Cell *83*. https://doi.org/10.1101/2021.09.10.459733.

64. Burrell, R.A., McClelland, S.E., Endesfelder, D., Groth, P., Weller, M.C., Shaikh, N., Domingo, E., Kanu, N., Dewhurst, S.M., Gronroos, E., et al. (2013). Replication stress links structural and numerical cancer chromosomal instability. Nature *494*, 492–496. https://doi.org/10.1038/nature11935.

65. Halliwell, J.A., Frith, T.J.R., Laing, O., Price, C.J., Bower, O.J., Stavish, D., Gokhale, P.J., Hewitt, Z., El-Khamisy, S.F., Barbaric, I., et al. (2020). Nucleosides rescue replication-mediated genome instability of human pluripotent stem cells. Stem Cell Rep. *14*, 1009–1017. https://doi.org/10.1016/j.stemcr.2020.04.004.

66. Patnaik, A., Rosen, L.S., Tolaney, S.M., Tolcher, A.W., Goldman, J.W., Gandhi, L., Papadopoulos, K.P., Beeram, M., Rasco, D.W., Hilton, J.F., et al. (2016). Efficacy and safety of Abemaciclib, an inhibitor of CDK4 and CDK6, for patients with breast cancer, non–small cell lung cancer, and other solid tumors. Cancer Discov. *6*, 740–753. https://doi.org/10.1158/2159-8290.CD-16-0095.

67. Kudo, R., Safonov, A., da Silva, E., Li, Q., Shao, H., Will, M., Fushimi, A., Nakshatri, H., Reis-Filho, J.S., Goel, S., et al. (2023). Long-term breast cancer response to CDK4/6 inhibition defined by TP53-mediated geroconversion. Preprint at bioRxiv. https://doi.org/10.1101/2023.08.25.554716.

68. Freund, A., Patil, C.K., and Campisi, J. (2011). P38MAPK is a novel DNA damage response-independent regulator of the senescence-associated secretory phenotype. EMBO J. *30*, 1536–1548. https://doi.org/10.1038/emboj.2011.69.

69. Purvis, J.E., Karhohs, K.W., Mock, C., Batchelor, E., Loewer, A., and Lahav, G. (2012). p53 dynamics control cell fate. Science *336*, 1440–1444. https://doi.org/10.1126/science.1218351.

70. Pang, Z., Chong, J., Zhou, G., de Lima Morais, D.A., Chang, L., Barrette, M., Gauthier, C., Jacques, P.É., Li, S., and Xia, J. (2021). MetaboAnalyst 5.0: narrowing the gap between raw spectra and functional insights. Nucleic Acids Res. *49*, W388–W396. https://doi.org/10.1093/nar/gkab382.

71. Cooper, S., Barr, A.R., Glen, R., and Bakal, C. (2017). NucliTrack: an integrated nuclei tracking application. Bioinformatics *33*, 3320–3322. https://doi.org/10.1093/bioinformatics/btx404.

72. Mirchandani, A.S., Jenkins, S.J., Bain, C.C., Sanchez-Garcia, M.A., Lawson, H., Coelho, P., Murphy, F., Griffith, D.M., Zhang, A., Morrison, T., et al. (2022). Hypoxia shapes the immune landscape in lung injury and promotes the persistence of inflammation. Nat Immunol *23*, 927–939. https://doi.org/10.1038/s41590-022-01216-z.

73. Creek, D.J., Jankevics, A., Burgess, K.E.V., Breitling, R., and Barrett, M.P. (2012). IDEOM: an Excel interface for analysis of LC–MS-based metabolomics data. Bioinformatics *28*, 1048–1049. https://doi.org/10.1093/bioinformatics/bts069.

74. Smith, C.A., Want, E.J., O'Maille, G., Abagyan, R., and Siuzdak, G. (2006). XCMS: processing mass spectrometry data for metabolite profiling using nonlinear peak alignment, matching, and identification. Anal. Chem. *78*, 779–787. https://doi.org/10.1021/ac051437y.

75. Chokkathukalam, A., Jankevics, A., Creek, D.J., Achcar, F., Barrett, M.P., and Breitling, R. (2013). mzMatch–ISO: an R tool for the annotation and relative quantification of isotope-labelled mass spectrometry data. Bioinformatics *29*, 281–283. https://doi.org/10.1093/bioinformatics/bts674.

76. Sumner, L.W., Amberg, A., Barrett, D., Beale, M.H., Beger, R., Daykin, C.A., Fan, T.W.-M., Fiehn, O., Goodacre, R., Griffin, J.L., et al. (2007). Proposed minimum reporting standards for chemical analysis chemical analysis working group (CAWG) metabolomics standards initiative (MSI). Metabolomics *3*, 211–221. https://doi.org/10.1007/s11306-007-0082-2.

77. Lord, S.J., Velle, K.B., Mullins, R.D., and Fritz-Laylin, L.K. (2020). SuperPlots: communicating reproducibility and variability in cell biology. J. Cell Biol. *219*. https://doi.org/10.1083/JCB.202001064.

78. Wiśniewski, J.R., Hein, M.Y., Cox, J., and Mann, M. (2014). A "Proteomic Ruler" for Protein Copy Number and Concentration Estimation without Spike-in Standards*. Molecular & Cellular Proteomics *13*, 3497–3506. https://doi.org/10.1074/mcp.M113.037309.

STAR★METHODS

KEY RESOURCES TABLE

REAGENT or RESOURCE	SOURCE	IDENTIFIER
Antibodies		
Rabbit monoclonal anti-p21	ThermoFisher	Cat. MA5-14949
Mouse anti-p21	BD	Cat. 556430
Rabbit anti-gamma H2AX (Ser139(	Cell signalling	Cat. 2577
Rabbit anti-53BP1	Cell signalling	Cat. 4937
Rabbit anti-p53	Cell signalling	Cat. 9282
Mouse monoclonal anti-Tubulin (clone DM1A)	Sigma	Cat. T6199
Rabbit monoclonal anti-p38	Cell Signalling	Cat. 8690S
Rabbit monoclonal anti-phospho-T180/ Y182 p38	Cell Signalling	Cat. 4511S
Rabbit anti-phospho-S15 HSP27	Cell Signalling	Cat. 2401S
Rabbit anti-Histone H3	Abcam	Cat. ab1791
Rabbit monoclonal anti-NQO-1	Cell Signalling	Cat. 62262
AlexaFluor 647 IgG goat anti-rabbit	ThermoFisher	Cat. A21245
AlexaFluor 488 IgG goat anti-rabbit	ThermoFisher	Cat. A11008
AlexaFluor 647 IgG goat anti-mouse	ThermoFisher	Cat. A21235
AlexaFluor 488 IgG goat anti-mouse	ThermoFisher	Cat. A11001
AlexaFluor 594 IgG goat anti-mouse	ThermoFisher	Cat. A-11032
Mouse Anti-BrdU (Clone 44)	BD	Cat. 347580
Rat Anti-BrdU	Abcam	Cat. ab6326
Chemicals, peptides, and recombinant proteins		
Palbociclib (PD0332991)	MedChemExpress	Cat. HY-50767A
Palbociclib (PD0332991)	Merck	PZ0383
Rapamycin	MedChemExpress	Cat. AY-22989
p38 inhibitor (SB-203580)	MedKoo	Cat. 574872
p38 inhibitor (SB-203580)	Merck	559389
p38 inhibitor (VX-745)	Tocris	3915
p38 inhibitor (BIRB-796)	Tocris	5989
JNK-I-8	Merck	SML1246
S-Trityl-L-cysteine (STLC)	Merck/Sigma	164739
TBE-31	Dinkova-Kostova lab	N/A
SPiDER-Bgal	Dojindo	SG03-10
N-acetyl cysteine (NAC)	Merck	A7250
CldU	Sigma	C6891
IdU	Sigma	I7125
Critical commercial assays		
IL-6 ELISA kit	R&D Systems	D6050
CCL2 ELISA kit	R&D Systems	DCP00
EdU Click-iT cell proliferation kit – Alexa 647 dye	ThermoFisher	C10337
Deposited data		
Proteomics dataset	PRIDE	PRIDE: PXD036519
Metabolomics dataset	MetaboLights	MetaboLights: MTBLS5868, MetaboLights: MTBLS8698

(*Continued on next page*)

Continued

REAGENT or RESOURCE	SOURCE	IDENTIFIER
Experimental models: Cell lines		
hTERT-RPE1 mRuby-PCNA	Jorg Mansfeld	Zerjatke et al.[32]
hTert-RPE1 mRuby-PCNA p21-GFP		Barr et al.[31]
hTert-RPE1 mRuby-PCNA p21KO1A		Barr et al.[31]
PCNA p21-GFP H3.1-iRFP	This study	N/A
hTERT-RPE1-FUCCI		Krenning et al.[28]
MCF7	ATCC	HTB-22
hTERT-RPE1	ATCC	CRL-4000
Software and algorithms		
Spectronaut	Biognosys	v.14.7.201007.47784
MetaboAnalyst	Pang et al.[70]	v5.0
NucliTrack	Cooper et al.[71]	N/A

RESOURCE AVAILABILITY

Lead contact

- Further information and requests for resources and reagents should be directed to and will be fulfilled by the lead contact, Tony Ly (tly@dundee.ac.uk).

Materials availability

- Cell lines generated in this study (see Key Resources Table) are available upon request.

Data and code availability

- Proteomics and metabolomics data have been deposited to the repositories PRIDE and MetaboLights, respectively, with accessions listed in the key resources table.
- The paper does not report original code.
- Any additional information required to reanalyze the data reported in this paper is available from the lead contact upon request.

EXPERIMENTAL MODEL AND STUDY PARTICIPANT DETAILS

hTERT-RPE1 mRuby-PCNA cells were a generous gift from Jörg Mansfeld (Institute of Cancer Research, London) and their generation is described in.[32] hTert-RPE1 mRuby-PCNA p21-GFP and hTert-RPE1 mRuby-PCNA p21KO1A were previously described in.[31] hTert-RPE1 mRuby-PCNA p21-GFP H3.1-iRFP cells were generated using AAV-mediated recombination to label endogenous Histone H3.1 (locus *HISTH31E*) at the C-terminus, as described in.[32] hTERT-RPE1-FUCCI cells were published previously.[28] MCF7 cells were from ATCC. Both MCF7 and hTERT-RPE1 are cell lines of female origin. Cell lines were maintained in DMEM (41966; Gibco) supplemented with 10% heat-inactivated FBS and 1% penicillin-streptomycin (both from Sigma) at 37°C and 5% CO2. Cells were screened for mycoplasma by PCR every 1–2 months. hTERT-RPE1 cells (ATCC) were also maintained in 1:1 DMEM/F-12 (10565018, Thermo) supplemented with 9% FBS (10270106, Thermo). Because RPE1 cells treated with CDK4/6i became fragile after 4 days treatment, experiments requiring cell dissociation were performed at day 4 of treatment.

METHOD DETAILS

Fixed-cell experiments to analyze release from CDK4/6 inhibitors

Cells were plated on black 384-well CellCarrierUltra (PerkinElmer) plates one day before adding inhibitors at a density of $2.5x10^4$ cells/ml in 20 μl of media/well. After cells had been incubated in inhibitors for the required number of days, depending on the experiment, inhibitor containing media was aspirated and cells washed four times in PBS, using an automated liquid handler – 50TS microplate washer (Biotek). Fresh media was then added to cells containing 10 μM EdU, in order to label cells as they enter S-phase. After 24 or 48h further incubation, cells were fixed and immunostained, as described below.

Fixed-cell experiments to quantify DNA damage after release

Cells were plated at a concentration of $1x10^4$ cells/ml in 6 well plates. After 6hr, when cells had attached, inhibitors were added to cells for seven days, with media and inhibitors being refreshed after 3 days. After seven days, inhibitors were washed from cells by washing four times in PBS, cells were trypsinised, resuspended in fresh media, centrifuged at 1,000xg for 3 mins, media aspirated, cells resuspended in 2ml of fresh media and 40ul of media was plated per well of a black 384-well CellCarrierUltra (PerkinElmer). Cells were left for 48h to release, then fixed and immunostained, as described below.

Fixed-cell experiments to quantify protein levels after inhibitor treatment

Cells were plated on black 384-well CellCarrierUltra (PerkinElmer) plates one day before adding inhibitors at a density of $1.25x10^4$ cells/ml in 20 μl of media/well. After cells had been incubated in inhibitors for the required number of days, cells were fixed and immunostained, as described below.

Immunofluorescence

For immunostaining in 384 well plates, cells were fixed by adding and equal volume of 8% formaldehyde in PBS to media in wells to give a final concentration of 4% formaldehyde. Cells were fixed for 15 minutes at RT and washed three times with PBS. Permeabilization in PBS 0.5% Triton X-100 for 15 min was followed by blocking in 2% BSA in PBS (blocking buffer) for 1 h. Cells were incubated with primary antibodies diluted in blocking buffer at 4°C overnight and washed three times with PBS, then incubated with a 1:1000 dilution of Alexa-labelled secondary antibodies (ThermoFisher), also diluted in blocking buffer for 1h at RT. Finally, cells were incubated with Hoechst 33258 (1ug/ml) for 15 min at RT, followed by 3 washes in PBS. All washes and aspirations were performed on the automated liquid handler (50TS microplate washer (Biotek)). Primary antibodies used for immunostaining in this study were: p21 (BD 556430, 1:500), p21 (Invitrogen MA5-14949: 1:1000), p53 (CST 2527, 1:500), gammaH2AX (CST 2577, 1:2000), 53BP1 (CST 4937,1:1000).

For EdU staining, a final concentration of 10 μM EdU was added to growth media. After fixing, permeabilising and blocking (as detailed above), the Click-iT reaction was performed as follows: cells were incubated in the dark, for 30 min at RT in a solution of 100 mM Tris-HCl pH 7.5, 4 mM CuSO4, 5 μM sulfo-cyanine-3-azide and 100 mM sodium ascorbate. Cells were then washed three times in PBS, and either immunostained with primary and secondary antibodies (detailed above) or directly incubated for 15 min at RT with 1 μg/ml Hoechst 33258, and then washed three times in PBS.

For the B-gal assay to detect senescence, cells were treated for 7d with inhibitors and then fixed in 4% formaldehyde for 20 min at RT. Fixed cells were then washed and incubated with SPiDER-Bgal reagent (Dojindo) for 30 min at 37°C. Cells were then washed 3 times in PBS and incubated with Hoechst 33258 (1ug/ml) for 15 min at RT, followed by 3 washes in PBS.

Fixed cell imaging of 384 well plates was performed on the Operetta CLS (PerkinElmer) high-content microscope using the 20x N.A. 0.8 objective.

Live imaging

CDK4/6i release experiments

hTert-RPE1 Ruby-PCNA or hTert-RPE1 Ruby-PCNA p21-GFP H3.1-iRFP cells were seeded at a density of $2.5x10^4$ cells/ml in 20 μl of media/well in 384-well CellCarrier Ultra plates (PerkinElmer) or 8-well Ibidi chambers one day before adding inhibitors. After 7d incubation in inhibitors, wells were washed four times in PBS and inhibitor-containing media was replaced with fresh phenol-red free DMEM with 10% FBS and 1% P/S before live imaging was started. Live imaging was performed on either the Operetta CLS high-content microscope (PerkinElmer) at 20x N.A. 0.8 in confocal mode or the Olympus ScanR confocal microscope at 20x N.A. 0.7. In both cases, cells were imaged under climate-controlled conditions at 37°C and 5% CO_2. Cells were acquired every 10 or 12 mins. To quantify the timing of release and subsequent cell cycle phase lengths, experiments were analysed manually using FIJI. To quantify p21-GFP levels after release, images were analysed using Nuclitrack.[71] For RPE1-FUCCI movies, cells were seeded at a low density (approximately 15,000 cells per well) and treated with CDK4/6i. Drug washout was performed 6 times every 30mins in fresh full growth media with 10 μM of STLC to block mitotic exit. The single-cell FUCCI cell cycle profiles were generated manually by analysing RPE1-FUCCI movies. A total of 50 red (G1 arrested) cells were randomly selected and marked at the beginning of the movie. The time points in which the FUCCI cells change colour was recorded to determine the time spent in each phase of the first cell cycle following release from CDK4/6 inhibition. RPE-FUCCI cells were always imaged with the same illumination settings and all images were placed on the same scale prior to analysis to ensure that the red/yellow/green cut-offs were reproducibly calculated between experiments. Mitotic entry was timed based on the visualization of typical mitotic cell rounding and loss of nuclear mAG-geminin signal. Note that we previously observed that STLC addition can lead to an increased fraction of cells re-entering S-phase after drug washout.[24]

p21-GFP quantification experiments

To quantify p21-GFP levels after addition of inhibitors to asynchronous cells, cells were plated in phenol-red free DMEM (10% FBS, 1% P/S) at a density of $2.5x10^4$ cells/ml in 20 μl of media/well, one day prior to the start of the experiment. The next day, inhibitors were added and media made up to a final volume of 100ul per well. Imaging was started immediately on the Operetta CLS microscope in confocal mode (PerkinElmer), using 20x N.A. 0.8 and acquiring images every 10-12 mins. Cells were maintained at 37°C and 5% CO_2 throughout imaging. To quantify p21-GFP levels after inhibitor additiong, images were analysed using Nuclitrack.[71]

Immunofluorescence flow cytometry

Cells were fixed in 2% formaldehyde for 15 min at 37 °C, washed in flow buffer (1% BSA in DPBS), and resuspended in ice-cold 90% methanol. For immunostaining, methanol-treated cells were washed with flow buffer, resuspended in immunostain solution containing 1:50 anti-p21 AlexaFluor 647 conjugate (Cell Signaling Technologies, #8587) in flow buffer and incubated at RT for 30 min. Cells were then washed with flow buffer and assayed using a Novocyte flow cytometer (ACEA Biosciences).

Modulation of extracellular osmolarity

DMEM/F12 was diluted 1:1 with sterile water and supplemented with sodium bicarbonate to 29 mM final (Thermo 25080094). Hypo-osmotic (179 mOsm/kg), isotonic (300 mOsm/kg) and hyper-osmotic (703 mOsm/kg) media was prepared by adding varying amounts of D-sorbitol (Sigma S1876). Flow cytometry analysis was performed as described above. Immunofluorescence microscopy was performed by culturing RPE1 cells on N1.5 13 mm coverslips (VWR), fixing cells with 4% formaldehyde (Thermo) at 37 °C for 15 min, permeabilizing with 0.1% Triton for 5 min, blocking with 1% BSA in TBS, incubating with primary antibody (1:200 dilution in 1% BSA in TBS) for 16 hr at 4°C, and then incubating with secondary antibodies (1:200 dilution in 1% BSA in TBS). Cells were then stained with DAPI, mounted on glass slides using ProLong Glass (Thermo) and imaged using a DeltaVision microscope (Imsol). Antibodies used were anti-p21 (CST #2947), anti-tubulin (DM1A, Merck), goat anti-rabbit AlexaFluor 555 (abcam, ab150078) and donkey anti-mouse AlexaFluor 488 (Thermo, A32766).

Cell volumes were measured using a HoloMonitor M4 in either Sarstedt Lumox, or Ibidi μ-plate glass-bottomed 24 well plates and the associated hololids. Optical volumes were determined using the holomonitor app suite.

Proteomics

Cells were scraped in 2% SDS lysis buffer containing phosphatase inhibitors (PhosStop, Roche) and protease inhibitors (Complete EDTA-free, Roche). Extracts were heated to 95 °C, cooled to room temperature, and treated with benzonase (Millipore, 70664) for 30 min at 37 °C. The benzonase treatment was repeated until the extract was free flowing. The protein concentration was determined and 50 μg protein aliquots were precipitated using acetone-ethanol. Precipitated protein was then digested with trypsin (1:100), once for 16 hours before another aliquot of trypsin is added (1:100) and incubated for an additional 4 hours. Peptides were then desalted using SepPak cartridges (Waters).

Peptides were analyzed by LC-MS/MS using a data-independent acquisition (DIA) approach implemented on a RSLCnano HPLC (Dionex) coupled to an Orbitrap Exploris 480 mass spectrometer (Thermo) using a DIA windows reported previously.[72] Peptides were separated on a 50-cm (2-μm particle size) EASY-Spray column (Thermo Fisher Scientific), which was assembled on an EASY-Spray source (Thermo Fisher Scientific) and operated constantly at 50 °C. Mobile phase A consisted of 0.1% formic acid in LC–MS-grade water and mobile phase B consisted of 80% acetonitrile and 0.1% formic acid. Peptides were loaded on to the column at a flow rate of 0.3 μl min^{-1} and eluted at a flow rate of 0.25 μl min^{-1} according to the following gradient: 2–40% mobile phase B in 120 min and then to 95% in 11 min. Mobile phase B was retained at 95% for 5 min and returned back to 2% a minute after until the end of the run (160 min in total).

The spray voltage was set at 2.2 kV and the ion capillary temperature at 280 °C. Survey scans were performed at 15,000 resolution, with a scan range of 350–1,500 *m/z*, maximum injection time 50 ms and AGC target 4.5×10^5. MS/MS DIA was performed in the orbitrap at 30,000 resolution with a scan range of 200–2,000 *m/z*. The mass range was set to 'normal', the maximum injection time to 54 ms and the AGC target to 2.0×10^5. An inclusion mass list with the corresponding isolation windows was used as previously reported. Data for both survey and MS/MS scans were acquired in profile mode. A blank sample (0.1% TFA, 80% MeCN, 1:1 v:v) was run between each sample to avoid carryover.

Metabolomics

Untargeted metabolomics analyses were performed by liquid chromatography-mass spectrometry (LC-MS) on a Thermo Fusion or a Thermo qExactive Orbitrap mass spectrometer interfaced with a Thermo UltiMate 3000 RSLC system. Samples were injected on to a ZIC-pHILIC column (150 × 4.6 mm, 5μm; Merck SeQuant, Umea, Sweden) maintained at 40°C (Thermo Fusion) or 25°C (qExactive). Mobile phase A consisted of 20mM ammonium carbonate in water and mobile phase B consisted of acetonitrile. The percentage of mobile phase A was increased from 20% to 80% over 15 min and then to 95% held for 2 min before re-equilibration to the starting conditions over 9 min. The flow rate was 300 μL/min. The mass spectrometer was operated in polarity-switching mode over the mass to charge ratio (m/z) range 70-1000 at a resolution of 120,000 (Thermo Fusion) or 70,000 (Thermo qExactive). The raw LC-MS files were processed with IDEOM,[73] which uses the XCMS[74] and mzMatch[75] software in the R environment. The annotation of metabolites was based on matching to the accurate mass of compounds in the HMDB, LIPID MAPS, MetaCyc and KEGG databases integrated in IDEOM together with comparison to an in-house authentic standard mix that was run alongside the samples. Lists of annotated metabolites and their relative abundances in the biological groups were retrieved and subjected to statistical analysis using MetaboAnalyst 5.0.[70] Metabolite assignment confidences are assigned according to published recommendations.[76]

DNA Fibre assays

RPE1 or MCF7 cells were plated into 6-well culture dishes, and the next day either treated with DMSO or arrested in palbociclib (1 μM) in the presence or absence of rapamycin (100 nM) for 7 days. Cells were then released into drug-free media for 16 hrs in the presence

and absence of EmbryoMax nucleosides (1x), then pulse-labelled with 25 μM CldU (Sigma-Aldrich) and 250 μM IdU (Sigma-Aldrich) for 15 min each. Cells were resuspended in PBS at 7.5 × 10^5 cells/ml. Then, 2.5 μl of cells was mixed with 7.5 μl of lysis buffer [200 mM Tris (pH 7.5), 25 mM EDTA, and 0.5% SDS] on a clean slide (Thermo Fisher Scientific). After 7 min, the slides were tilted at 25° and then air-dried, before fixation in methanol/acetic acid (3:1). DNA fibres were denatured using 2.5 M HCl for 75 min and then washed extensively with 1× PBS before blocking in 1% bovine serum albumin (BSA)/PBS containing 0.2% Tween-20 for 1 hour. CldU- and IdU-labeled tracts were incubated with two anti-BrdU (5-bromo-2′-deoxyuridine) antibodies (one specific for CldU (Abcam) and the other for IdU (BD)), washed, and incubated with goat anti-mouse/rat Alexa Fluor 488 and Alexa Fluor 594 (Invitrogen). DNA fibres were visualized on a Zeiss LSM710 confocal microscope, and images were collected using Zen software and then analysed with ImageJ.

IL-6 and CCL2 ELISA

IL-6 and CCL2 were measured using commercial kits (R&D Systems, D6050 and DCP00) in conditioned media over a 24 hour period. In brief, culture media was refreshed with new media 24 hours prior to harvesting supernatant. The kit protocol was followed, which included clearing the supernatant of cell debris by centrifugation and incubation with provided reaction buffers prior to microplate absorbance measurement at 450 nm wavelength (FLUOstar Omega, BMG Labtech).

QUANTIFICATION AND STATISTICAL ANALYSIS

Statistical details, including the statistical tests, the exact values of n, the definition of center, and dispersion/precision measures used can be found in figure legends.

Image quantification

All fixed cell image analysis was performed in Harmony automated image analysis software (PerkinElmer). Data were plotted in GraphPad Prism 7 and repeat experiments plotted as Superplots,[77] where appropriate.

Prior to all image analysis flatfield correction was applied in the Harmony software. To calculate nuclear intensities and cell and nuclear area, nuclei were identified and segmented based on Hoechst staining. Poorly segmented, nuclei at the edge of the field of view, mitotic and dead cells were excluded from analysis based on a combination of features measuring area, roundness and Hoechst intensity. Nuclear intensities and nuclear area were then quantified in well-segmented nuclei. Results displayed for fixed cell images show the mean nuclear intensity over all cells imaged in the well.

To calculate the percentage of EdU positive cells, EdU intensity was quantified in well-segmented nuclei. EdU positive cells were identified via setting a threshold based on the biphasic population.

To identify DNA damage foci with gammaH2AX or 53BP1 immunostaining, the spot finding function B of the Harmony software was used. Small foci labelled by these antibodies that are frequently visible in S-phase cells were excluded based on their smaller size and lower staining intensity.

For Figure S5F and H, violin plots were made using PlotsOfData (https://huygens.science.uva.nl/PlotsOfData). This allows the spread of data to be accurately visualized along with the 95% confidence intervals (thick vertical bars) calculated around the median (thin horizontal lines). Statistical comparison can then be made by eye between any treatment and time points, because when the vertical bar of one condition does not overlap with one in another condition, the difference between the medians is statistically significant ($P < 0.05$).

Proteomics Data Analysis

MS raw data files were processed using Spectronaut v.14.7.201007.47784 with a human reference FASTA sequence from UniProt, using default search parameters. The resulting protein-level data were analyzed using R v.3.5.0. Protein abundances are expressed as parts-per-million (ppm) and protein copies.[78] To calculate ppm, protein intensities were divided by the total protein intensity and therefore reflect a concentration.